Public Quarterly Report

Date of Report: *1st Quarterly Report, January 31, 2025*
Contract Number: *693JK32410012POTA*
Prepared for: *PHMSA*
Project Title: *Development of a Blade Toughness Meter (BTM) for In-situ Pipe Toughness Measurement*
Prepared by: *Massachusetts Materials Technologies*
Contact Information: *Simon Bellemare, s.bellemare@bymmt.com,*
For quarterly period ending: *December 31, 2024*

1: Items Completed During this Quarterly Period:

Table 1 shows a list of items that were completed this quarterly period. In addition to finishing Task 1.1 – Literature review, we began work on Task 1.2 – BTM Finite Element Model Development which is scheduled to be completed in approximately 12 months.

Table 1 – Tasks completed and invoiced this quarterly period

Item #	Task #	Activity/Deliverable	Title	Federal Cost	Cost Share
1	1.1	Literature Review - Research, summarize, and document current NDE and ILI fracture toughness measurement methods	A review report of current NDE and ILI methods and their technology readiness level submitted	$13,254.19	$16,719.09
3	N/A	1st Quarterly Report	Submit 1st quarterly report	0.00	0.00

2: Items Not-Completed During this Quarterly Period:

Table 2 shows a list of items for which work started during our first quarter but are not completed. Initial findings from work conducted in Quarter 1 for Task 1.2 was presented to the TAP committee on January 6, 2025. Progress for Task 1.2 is on track as originally defined in our proposal. Task 1.3 work has begun, and a progress report will be provided in the quarter 2 report.

Table 2 – Items started but not completed this quarterly period

Item #	Task #	Activity/Deliverable	Title	Federal Cost	Cost Share
2,4	1.2	Develop a finite element model for the planing-induced microfracture process	A report on findings from the finite element models which include (1) blade optimization design and (2) measurables and their correlations to fracture toughness submitted	$45,397.00	$45,397.50
5	1.3	Manufacture blades with optimized design and adjust tool accordingly	A summary of blade and tool design changes submitted	$21,535.66	$21,536.00

3: Project Financial Tracking During this Quarterly Period:

The total amount billed for completed work can be seen in Figure 1, along with a projected invoice schedule for the entire project. As described in Section 1, the only completed task is 1.1 – Literature Review. The total invoiced to PHMSA will be $13,254.19 as originally proposed in Attachment 3 of our initial proposal. We went slightly over budget for this task, which increased our cost share as shown in Table 1. Initial work began on Task 1.2 as discussed below in Section 4. Task 1.2 is expected to last approximately 12 months so no billing for this task occurred this quarter.

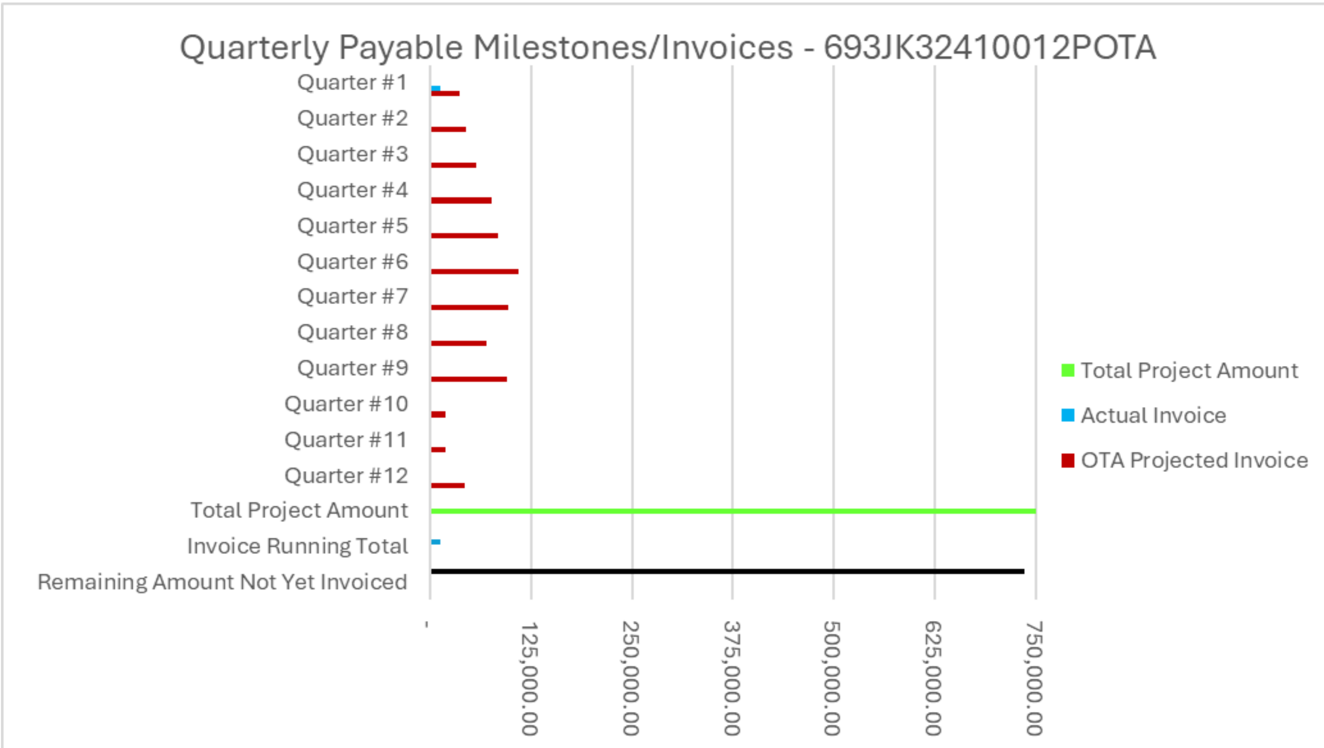

Figure 1 – MMT quarterly payable milestones and invoices

4: Project Technical Status –

Table 3 shows a complete summary of all project progress to date listed by Task as originally defined in our proposal. For each task we have listed the percentage achieved and percentage complete. A percentage achieved less than 100% with a percentage complete of 100% indicates we did not complete all tasks as defined in our original proposal but we are stopping all work associated with the task.

A final technical report for Task 1.1 – Literature Review and a progress report for Task 1.2 – BTM Finite Element Model Development can be found in attachments 1 and 2, respectively.

Table 3 – Complete project progress summary

Scope of Work			% Achieved	% Complete
Milestones	**Type**	**Tasks**		
Milestone 1: Blade Optimization for Better Accuracy and Safety	Deliverable	1.1 Literature Review	100	100
	Method	1.2 BTM Finite Element Model Development	25	25
	Hardware	1.3 Blade Design Optimization	0	0
Milestone 2: Field Trials and Evaluation	Hardware	2.1 Field Device Development	0	0
	Software	2.2 Data Process and Analytics Optimization	0	0
	Procedure	2.3 Field Procedure Optimization	0	0
	Deliverable	2.4 Third-Party Validation	0	0
Milestone 3: Test Instrument Design and Evaluation	Hardware	3.1 Field Device Optimization and Automation	0	0
	Software	3.2 Software Development	0	0
	Procedure	3.3 Training Program Development	0	0
	Deliverable	3.4 Engineering Specification for Manufacturing	0	0
Milestone 4: Proof-of-Concept for In-line Adaption	Method	4.1 Feasibility Study	0	0
	Hardware	4.2 Proof-of-Concept Development	0	0
	Deliverable	4.3 Laboratory Mock-up Testing	0	0

5: Project Schedule –

A complete project progress summary can be seen in Table 3. This summary includes all tasks that have not been started yet as well as percentage progress for ongoing tasks. It is anticipated that at the time of quarter 2 report submission that tasks 1.2 and 1.3 will each be approximately 50% complete.

Attachment 1 – Task 1.1 – Literature Review Report

Task 1.1 - Literature Review for
PHMSA Project: Development of the Blade Toughness Meter (BTM) for In-Situ Pipe Toughness Measurement (Project # 1043)
Author: Xuejun (Tony) Huang, PhD
Date: 01/15/2014

1. Introduction

The scope of the literature review is defined in the submitted proposal, and it covers three main topics: (1) the state of the art of non-destructive and ILI technologies for measuring fracture toughness. This will set the stage for the current project, comparing the BTM technology with existing and incoming technologies in the market; (2) Predictive models for pipe body ductile-brittle transition temperature (DBTT). This will be utilized to estimate the DBTT of a pipe before we perform the BTM testing in the field to make sure we always test a pipe in the ductile region at the testing temperature; (3) The dependence of laboratory K values on testing temperature. The learnings from this literature review will be utilized to normalize laboratory and field data taken at different temperatures. It will help the development of the machine learning prediction models, as well as the reporting of BTM results.

2. Methodology

In this literature review, the primary search engine utilized was Google Scholar. The selection of keywords was tailored to the specific topics of interest, commonly including terms such as 'fracture toughness,' 'correlation,' 'transition temperature,' and 'temperature effect.' Additionally, certain references were identified based on previous familiarity with the subject matter, such as conference papers previously encountered. All cited literature was published post-1970s to ensure the relevance and timeliness of the data. The inclusion criteria for sources focused exclusively on works discussing fracture toughness, with a preference for studies involving pipeline steels. However, the review was broadened to all metals with a focus on steel to provide a larger base of knowledge for the project. To guarantee the reliability of the sources, only references with a citation count exceeding 10 on Google Scholar were considered, except for four recently published papers from after 2021. Most of the selected sources had over 20 citations. For studies pertaining to specific technologies, efforts were made to identify and review the seminal papers that first introduced the concepts or initiated the experiments.

3. Thematic or Conceptual Organization of Findings

3.1 Non-destructive and ILI Technologies for Measuring Fracture Toughness

3.1.1 Ultrasonic Testing (UT)

Alex Vary at NASA Lewis Research Center (now Glenn Research Center) has conducted a series of studies to correlate UT measurements to material fracture toughness since the 1970s (Vary, 1978, 1979, 1982, 1989; Vary & Hull, 1982). In his report (Vary, 1978), he argued that fracture toughness (Kc) is intrinsically linked to a material's microstructure. Since the attenuation of ultrasonic waves (e.g., elastic waves) is also influenced by microstructure, it follows that Kc is related to the ultrasonic attenuation properties. Consequently, a correlation can be expected between fracture toughness and ultrasonic propagation characteristics.

In his experiment (Vary, 1978), broadband piezoelectric transducers (10–50 MHz) with fused quartz delay lines were used, coupled to the specimens with glycerin. Ultrasonic velocity was measured using a modified pulse-echo overlap method, while attenuation coefficients were determined through

differential spectral analysis of the first two back-surface echoes. An oscilloscope and signal-processing units analyzed the frequency spectrum and amplitude ratios of the ultrasonic signals.
By examining maraging steels (grades 200 and 250) and a titanium alloy (Ti-8Mo-8V-2Fe-3Al), he found a strong correlation between ultrasonic attenuation coefficient (derived from frequency spectrum analyses) and material toughness. The following correlation equation was proposed (Vary, 1979; Vary & Hull, 1982):

$$\left(\frac{K_{Ic}}{\sigma_y}\right)^2 = M\left(\frac{v_l\beta_\delta}{m}\right)^{0.5}$$

where K_{Ic} is the plain strain fracture toughness of the material, σ_y is the yield stress, M is a material constant, v_l is the longitudinal ultrasound velocity in the material. β_δ is defined as the derivative of the attenuation coefficient, α, over the frequency f, at a specific frequency of f_δ:

$$\beta_\delta = \left.\frac{d\alpha}{df}\right|_{f=f_\delta}, \text{and } f_\delta = v_l/\delta$$

where δ is a characteristic or critical dimension of the microstructural factor that governs the material fracture toughness. m is the exponential coefficient in the relation between attenuation coefficient and frequency:

$$\alpha = cf^m$$

Figure 1 shows the correlations obtained from experimental data for the three different materials.

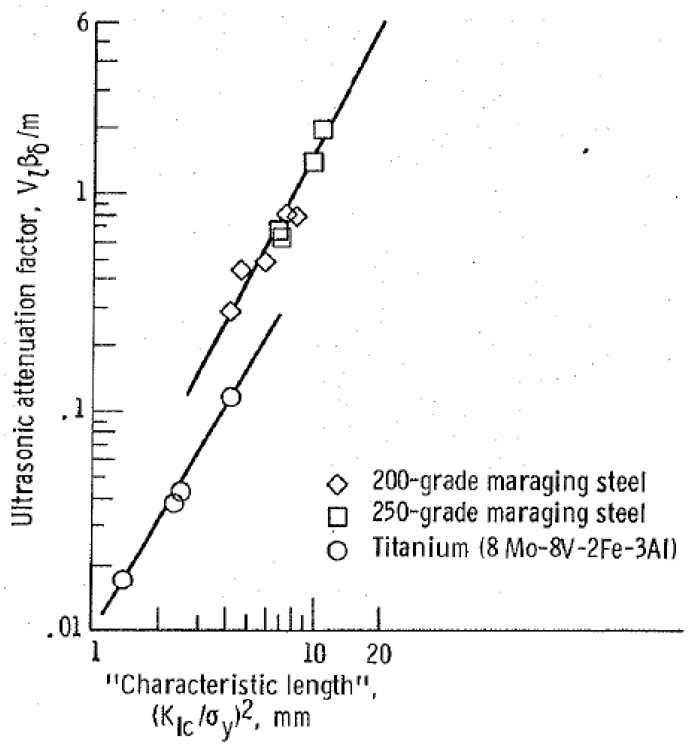

Figure 1 Experimental results showing predicted correlation of ultrasonic attenuation factor and fracture toughness (Vary, 1989).

Vary introduced three conceptual models - Stress Wave Interaction (SWI), Microstructure Transfer Function (MTF), and Microcrack Nucleation Mechanics (MNM) - to explain and predict the correlations between ultrasonic attenuation, microstructure, and fracture toughness in polycrystalline solids (Vary, 1989). These models provide insights into how ultrasonic attenuation measurements reflect material behavior during stress wave interactions at microstructural features and can be utilized to predict fracture toughness.

Following Vary's work, multiple papers have been published on using UT to measure fracture toughness of different materials (Gür & Yildiz, 2008; Gür & Yıldız, 2004; Jeong et al., 2003; Krüger et al., 1999; R. L. Smith & Reynolds, 1982; Williams et al., 2022).

Smith and Reynolds investigated the relationships among ultrasonic attenuation, microstructure, and the ductile-to-brittle transition temperature (DBTT) in very low carbon steels with 0.02 wt.% C (R. L. Smith & Reynolds, 1982). They analyzed how ultrasonic attenuation and DBTT varied with ferrite grain size and its distribution. The ultrasonic attenuation in these steels was found to be anomalously high compared to normal low-carbon steels, which the authors attributed to wide grain-size distributions and hysteresis losses, such as dislocation and magnetic domain wall damping. Larger ferrite grain sizes were associated with higher DBTT, indicating increased brittleness at room temperature. They identified an empirical correlation between DBTT and ultrasonic attenuation, noting that higher attenuation corresponded to higher DBTT and greater material brittleness. A parametric correlation of the DBTT with the ultrasonic attenuation parameter was found.

Krüger et al., explored the use of ultrasonic spectral analysis to detect hydrogen-induced damage in steel (Krüger et al., 1999). The study focuses on small cracks caused by hydrogen in H_2S environments, using ASTM A516 gr 60 steel samples. The samples were subjected to hydrogen attack under controlled conditions, and both ultrasonic and metallographic analyses were conducted to characterize the damage. Results showed that hydrogen-attacked samples exhibited distinct spectral characteristics, including higher attenuation at high frequencies and variations in the second-order moment of the spectrum. While specific toughness values were not measured, the study demonstrated that ultrasonic spectral analysis is a sensitive method for detecting hydrogen-induced embrittlement.

Gür and Yildiz explored the use of non-destructive techniques to assess the impact toughness of precipitation-hardened aluminum alloys. One study (Gür & Yıldız, 2004) focused on the 7020 Al–Zn–Mg alloy, aged at 140 °C following natural aging. Impact toughness decreased with aging time due to the formation of metastable η' precipitates, which increased hardness and brittleness. Sound velocity was inversely proportional to impact toughness (Figure 2). In another study (Gür & Yildiz, 2008), they examined the 2024 Al–Cu–Mg alloy, investigating the effects of aging at 190 °C. Results show that impact toughness initially increases, peaks after 3 hours, and then sharply declines after 7 hours due to the formation of coarse, incoherent precipitates. Similar to the findings for the 7020 alloy, sound velocity correlated with changes in impact toughness. The two studies demonstrate the potential of UT measurements in monitoring material properties during aging of aluminum alloys.

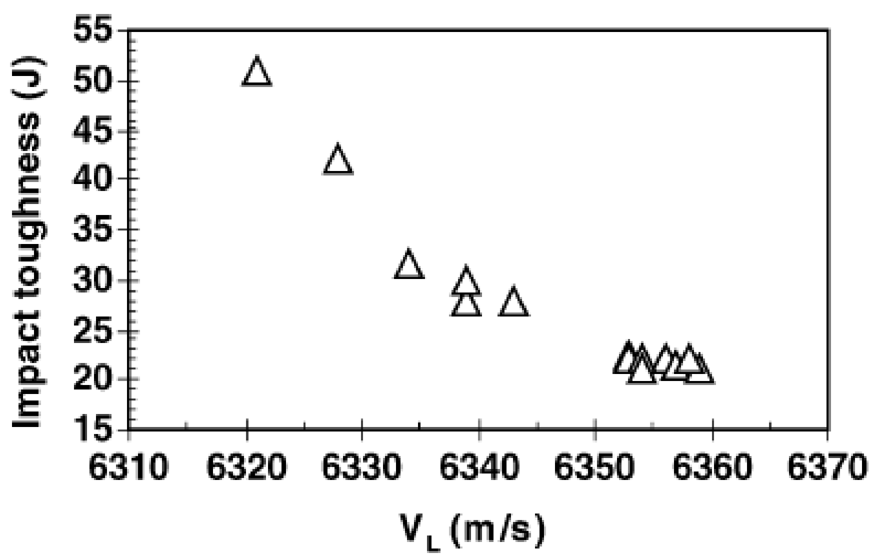

Figure 2 For the 7020 alloy specimens aged at 140 °C for various times following 96 h natural ageing, correlation between ultrasonic longitudinal wave velocity and impact energy (Gür & Yıldız, 2004).

Two recent studies explored the use of nonlinear ultrasonic testing as a nondestructive method for evaluating fracture toughness in steels. Jeong et al. investigated CrMoV rotor steels subjected to various aging times, employing second harmonic generation to measure the nonlinearity parameter (β) and correlating it with the fracture appearance transition temperature (FATT) (Jeong et al., 2003). FATT was then used to estimate fracture toughness through existing empirical relationships. The study demonstrated that β increased with aging time due to grain boundary segregation and embrittlement, effectively predicting fracture toughness (Figure 3). Similarly, Williams et al. applied nonlinear UT to 4130 steels with different heat treatments, comparing the β values with Charpy V-Notch (CVN) absorbed energy (Williams et al., 2022). The study analyzed bulk and surface wave modes, finding a monotonic relationship between β and absorbed energy for bulk waves, while surface waves exhibited non-monotonic trends due to sample heterogeneity. Both studies confirmed the sensitivity of nonlinear UT to microstructural changes, highlighting its potential as a nondestructive technique for monitoring toughness for steels.

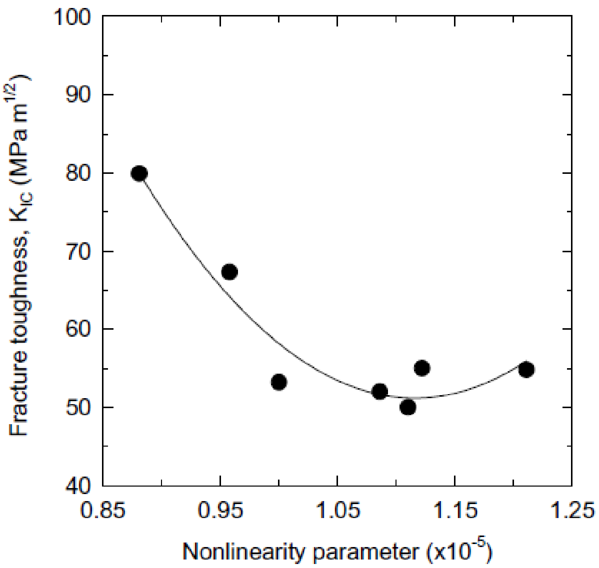

Figure 3 Correlations between the nonlinearity parameter (β) and the fracture toughness.

3.1.2 Instrumented Indentation Technology (IIT)

Haggag and Nanstad at Oak Ridge National Lab proposed a simple technique for estimating the fracture toughness by coupling the measured flow properties either from a uniaxial tensile test or from an automated ball indentation (ABI) test (Haggag & Nanstad, 1989):

$$K_{Ic} = C\left(\epsilon_u \cdot l_0^* \cdot E \cdot \sigma_y\right)^{0.5}$$

where K_{Ic} is the material initiation fracture toughness, C is a material constant, ϵ_u is the uniform elongation strain in a tensile test, l_0^* is a characteristic distance which is considered as a multiple of the planar inclusion spacing (which is measured to be 250 μm from SEM examination of a steel sample and assumed to be same for all steels studied in the paper), E is the Young's modulus and σ_y is the yield stress.

Tensile tests on A515 grade 70 steel and ABI tests on A533 grade B class 1 steel demonstrated that the predicted fracture toughness values deviated by less than 11% from experimental measurements.

Haggag et al. introduced the indentation energy to fracture (IEF) parameter as a nondestructive measure to characterize the ductile-to-brittle transition temperature (DBTT) in carbon steels (Haggag et al., 1998). IEF is calculated from the indentation load versus depth data using the following equation:

$$IEF = \int_0^{h_f} P_m(h)dh\,, where\ P_m = \frac{4P}{\pi d^2}$$

where P_m is the mean indentation contact pressure, P is the indentation load, h is the indentation depth, h_f is the indentation depth up to the cleavage fracture stress, and d is the chordal diameter of the indentation. The critical indentation depth (h_f) was determined from the true stress vs. indentation depth curve from ABI testing at a specific test temperature with a critical stress index (800 MPa). Results show a temperature dependence of IEF, which aligns with Charpy impact energy trends (Figure 4). The authors proposed replacing Charpy impact energy with the IEF index for nondestructive DBTT assessments in carbon steels.

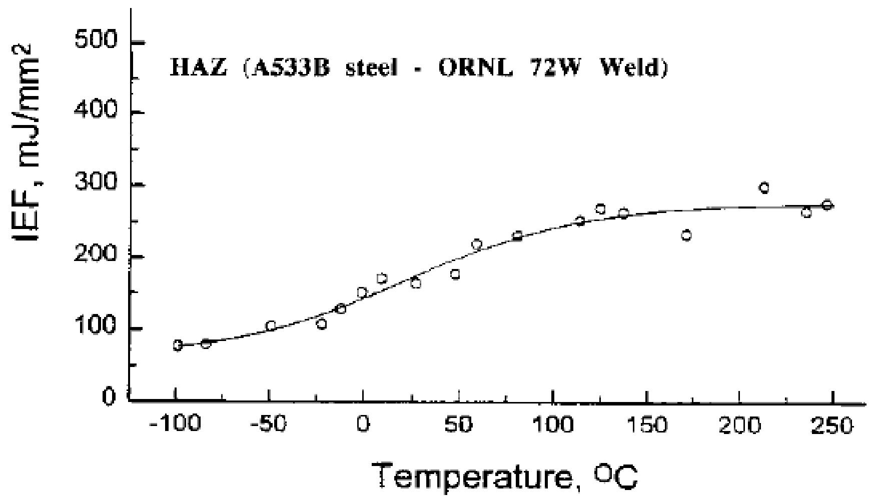

Figure 4 Temperature Variation of IEF for a heat affected zone of a weld (Haggag et al., 1998)

Byun and colleagues investigated methodologies for estimating fracture toughness in reactor pressure vessel (RPV) steels using ball indentation tests combined with theoretical models (Byun et al., 1998, 2000). They applied the concept of indentation energy to fracture (IEF) model and stress state analyses to predict fracture toughness and characterize transition behavior in ferritic steels. The authors proposed a model that related indentation deformation energy to fracture toughness (Byun et al., 1998):

$$\frac{K_{Ic}^2}{2E} = W_f = W_0 + W_T, where\, W_T = W_{IEF}$$

where K_{Ic} is the material fracture toughness, E is the Young's modulus, and W_f is fracture energy per unit area which is considered to be composed of two parts: a lower shelf energy per unit area (W_0), determined by the fracture surface formation energy and pure elastic energy and a temperature-dependent energy (W_T). The authors further assumed that the W_T could be estimated using the indentation energy to fracture (W_{IEF}) since W_{IEF} includes only elastic–plastic deformation energy. The critical indentation depth was identified using a critical stress criterion. The predicted results using indentation method follow the trend of the ASTM master curve. The reference temperature, T_0, obtained by regression of the estimated K_{Ic} data, linearly correlates to the Charpy reference temperature, T_{41J}, measured from CVN testing.

The authors also conducted a finite element simulation to analyze the stress and strain fields during indentation. They reported that the stress triaxiality at the center of the indentation impression was similar to that observed ahead of a crack tip (Figure 6).

Using the same technique, the authors examined more reactor vessels steels and obtained similar results (Byun et al., 2000).

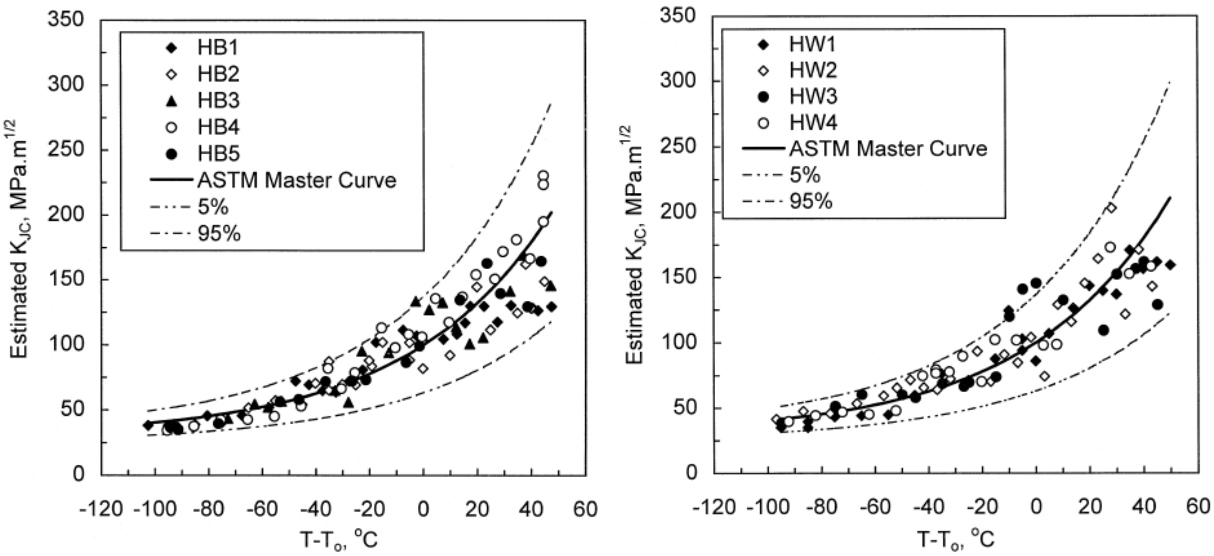

Figure 5 Estimated fracture toughness of SA508 Gr.3 steel base metals (left) and SA508 Gr.3 steel weld metals (right) (Byun et al., 1998).

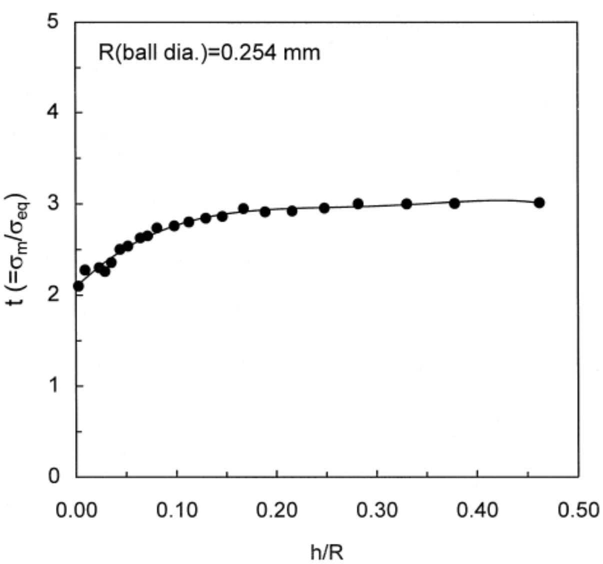

Figure 6 Variation of stress triaxiality at the center of impression with normalized indentation depth (t – triaxiality, h - indentation depth. R – ball indenter radius) (Byun et al., 1998).

Lee et al. proposed a model to correlate the indentation energy to fracture with fracture toughness by leveraging continuum damage mechanics (CDM) to identify the characteristic fracture initiation point during the indentation process (Lee et al., 2006). The concept of a critical void volume fraction was introduced, with a critical value of 0.25 determined through a literature review. It was assumed that damage beneath the indenter, such as voids nucleated in ductile materials, increases with indentation depth, leading to a decrease in Young's modulus. Based on the critical void volume fraction for crack initiation, the critical level of damaged Young's modulus was calculated to be 0.52 of the undamaged value. Using indentation testing, a curve of damaged Young's modulus (E_D) versus indentation depth (h) was obtained. By linearly extrapolating this curve to the critical damaged Young's modulus, the critical indentation depth and corresponding critical indentation energy were determined (Figure 7). The predicted fracture toughness values for several pipeline steels were compared with laboratory measurements obtained from CTOD tests, demonstrating good agreement (Figure 8).

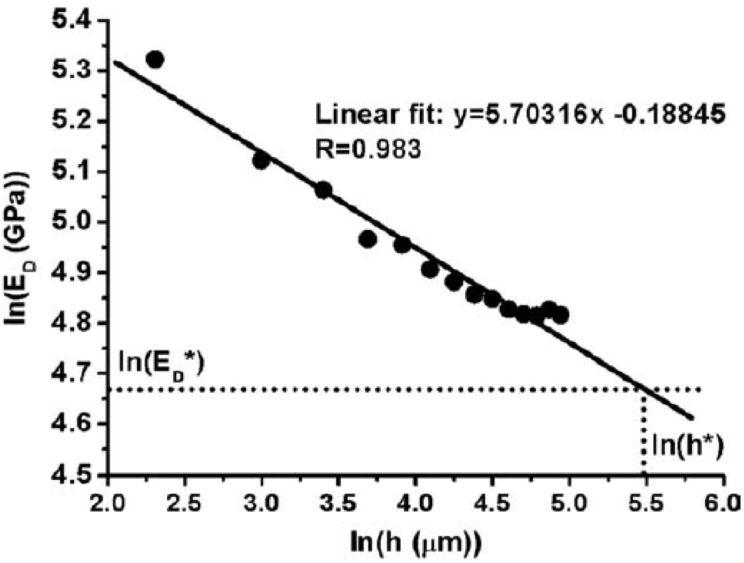

Figure 7 Relation between damaged Young's Modulus (E_D) and indentation depth (h) for API X7 (Lee et al., 2006).

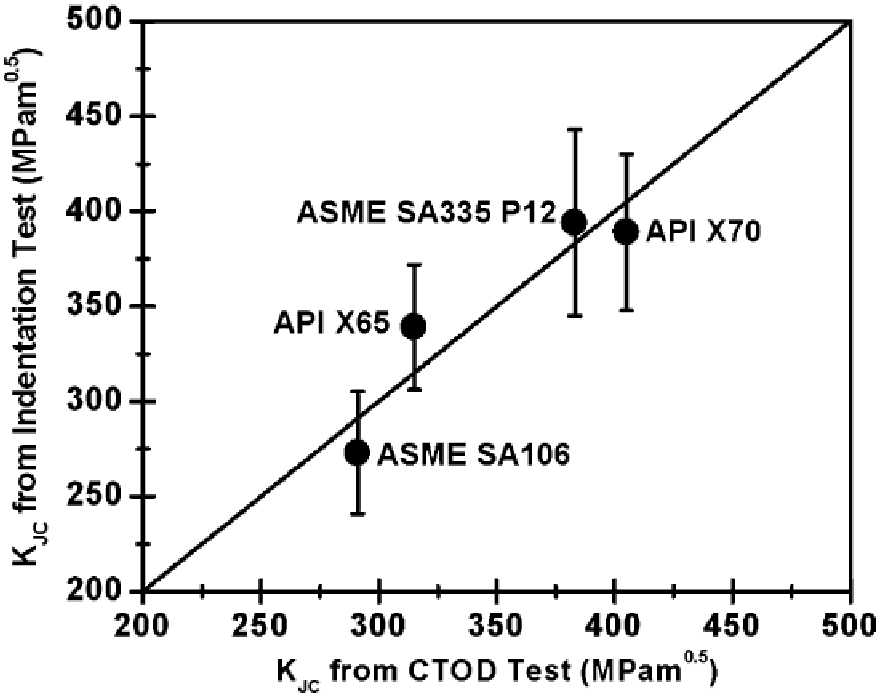

Figure 8 Comparison of fracture toughness measured in CTOD tests and predicted using indentation tests ((Lee et al., 2006).

Jeon et al. proposed a method for estimating the fracture toughness of metallic materials using instrumented indentation testing (Jeon et al., 2017). The proposed method incorporates two models: a critical indentation stress model for brittle materials (K_{Ic}<100 MPa√m) and a critical indentation strain model for ductile materials (K_{Ic}>250 MPa√m). For brittle materials, the critical mean pressure, defined as the criterion for crack extension, was derived from contact mechanics and determined to be 4.83 times the yield stress of the material. For ductile materials, the strain-based model utilized an empirical correlation between engineering fracture strain and uniform elongation, with the latter approximated using the hardening exponent obtained from indentation tests.

The methodology was validated through experiments on 27 metallic materials, comparing results from instrumented indentation testing with those from conventional fracture toughness tests. The authors conclude that the indentation-based approach provides fracture toughness estimates with variations of approximately 15% for brittle materials (Figure 9) and 20% for ductile materials (Figure 10) compared to standard tests. The outliers in Figure 10 were identified as materials in the transition region where the proposed models were less effective. A significant factor in obtaining a correlation is the broad range of alloys used for the study. With the yield strength as an key input parameter and the experimental yield strength varying from the low values for aluminum and mild steel to high values such as API X120 as an example, a correlation is not surprising.

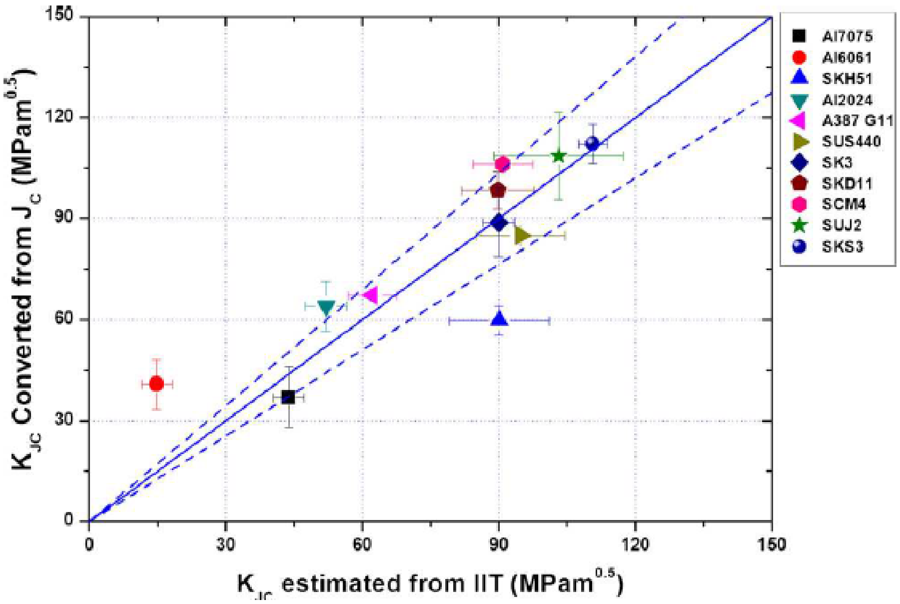

Figure 9 Comparison of the fracture toughness in the fracture tests and indentation tests of brittle metallic materials (the dotted lines indicate a deviation of 15 %) (Jeon et al., 2017).

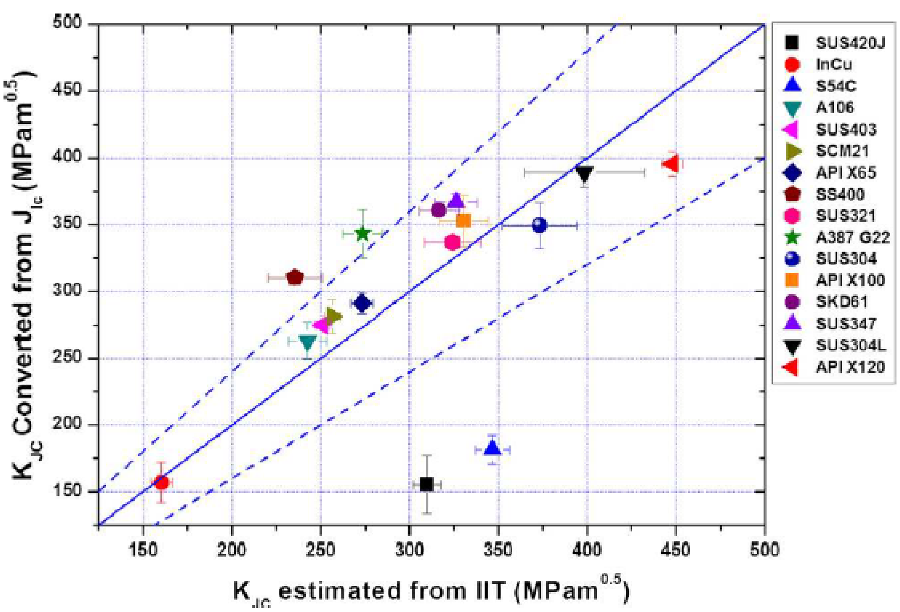

Figure 10 Comparison of the fracture toughness in the fracture tests and indentation tests of ductile metallic materials (the dotted lines indicate a deviation of 20 %) (Jeon et al., 2017).

Ted L. Anderson critiqued the claims by others that instrumented indentation testing can reliably measure fracture toughness in metallic materials (Anderson, 2023). While the method is widely recognized for determining strength properties such as yield and tensile strength, the author argued that it is fundamentally flawed as a technique for toughness measurement.

The paper highlights the distinction between engineering fracture strain (or elongation at break) and true fracture strain, emphasizing that the latter is crucial for assessing fracture toughness but is challenging to measure from conventional tensile tests due to necking phenomena. Similarly, indentation tests cannot determine true fracture strain, as necking and cracking do not occur during the indentation process. As a result, the plastic flow properties measured during indentation are fundamentally decoupled from the fracture properties of materials, rendering it impossible to accurately infer fracture toughness.

The author critically evaluated the ductile material model proposed by Jeon et al. (Jeon et al., 2017), which estimates fracture toughness using uniform elongation data derived from indentation tests. Anderson demonstrated that applying the same equation to estimate fracture toughness but substituting uniform elongation values from tensile tests (also provided in Jeon's study), resulted in significantly inaccurate toughness predictions. Additionally, the author identified several flaws in Jeon's brittle material model, notably its failure to account for the importance of stress distribution in cleavage fracture. Cleavage fracture is influenced not only by peak stress but also by the distribution of cleavage triggers, such as inclusions, which the model overlooked. The study concludes that while instrumented indentation is a useful tool for measuring strength properties, its application to toughness estimation is unsupported and unreliable.

3.1.3 Cutting Method (CM)

A.G. Atkins explored the integration of ductile fracture mechanics into metal cutting analysis, offering new insights into how cutting processes can be used to estimate fracture toughness (Atkins, 2003). Unlike traditional theories, such as the Ernst-Merchant model, which focus on plasticity and friction, Atkins emphasized the critical role of surface energy in metal cutting. He analytically that the work required for surface formation, often in the kJ/m² range for ductile metals, can be used to infer material fracture toughness through careful analysis of cutting forces and chip formation. A revised version of cutting force equation was proposed:

$$F_c V = (\tau_y \gamma)(t_0 w V) + [F_c \sec(\beta - \alpha) \sin\beta] \frac{V \sin\phi}{\cos(\phi - \alpha)} + RwV$$

where F_c is the horizontal component of the cutting force, V is the cutting velocity, τ_y is the shear yield stress of the material, γ is the shear strain along the shear plane, given by $\gamma = \cot\phi + \tan(\phi - \alpha)$; t_0 is the uncut chip thickness, w is the width of the orthogonal cut, β is the friction angle given by $\tan\beta = \mu$, with μ the coefficient of friction, α is the tool rake angle, ϕ is the orientation of the shear plane, and R is the specific work of surface formation which Atkins also called fracture toughness. The first and second terms on the right-hand side represent the shear and friction energy, while the third term is newly added and represents the surface formation energy.

The above equation can be rewritten as follows:

$$F_c = \left(\frac{\tau_y w \gamma}{Q}\right) t_0 + \frac{Rw}{Q}$$

where $Q = [1 - \sin\beta \sin\phi / (\cos(\beta - \alpha) \cos(\phi - \alpha))]$. When t_0 is large enough to make the dimensionless parameter $Z = R/(\tau_y * t_0) < 0.1$, the bracketed term before t_0 is constant. Hence, under this condition F_c is predicted to vary linearly with t_0. The incorporation of fracture toughness into the cutting model predicts a positive intercept in cutting force versus depth plots, effectively addressing the size effect observed in traditional cutting models (Figure 11).

Atkins calculated the R values from cutting experiment data found literature and compared them to J-integral values obtained from traditional fracture toughness tests (Figure 12). The two values for a given material did not match, which Atkins attributed to the effects of high strain rates and/or elevated temperatures during the cutting process.

Atkins' study establishes a framework where the intercepts in cutting force versus depth plots become an indicator of material fracture toughness. This approach provides a nondestructive method for assessing toughness directly from cutting experiments.

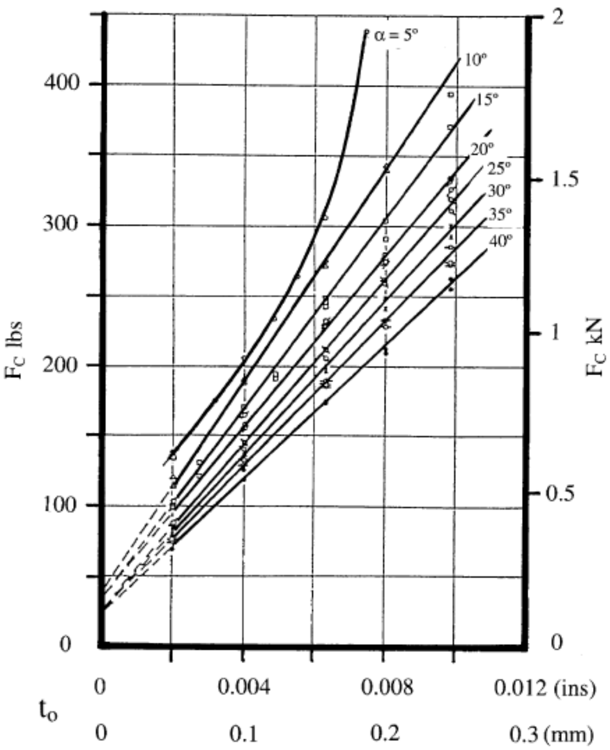

Figure 11 Cutting force vs. depth of cut for SAE 1112 cold rolled steel (Atkins, 2003).

Materials	R/τ_y (m)	τ_y (MPa)	R (kJ/m^2)	Independent quasi-static R[a,b] (kJ/m^2)
Annealed SAE 1112 steel[c]	4×10^{-5}	445	18	200
Cold worked SAE 1112 steel[c]	3×10^{-5}	571	16	200
"Mild steel"[d]	6×10^{-4}	—	—	300
"Steel"[e]	3×10^{-3}	—	—	—
SAE 4135 steel[f]	3×10^{-5}	570	18	60
NE 9445 steel[g]	2×10^{-5}	583	14	—
SAE 1015 steel[h]	4×10^{-5}	683	24	—
2024-T4 aluminium alloy[c]	2×10^{-5}	350	6	15
6061-T6 aluminium alloy[c]	3×10^{-5}	239	7	30
"Aluminium"[d]	5×10^{-3}	—	—	—
"Aluminium"[e]	2×10^{-3}	—	—	—
85/15 cold drawn brass[c]	3×10^{-5}	354	11	250
"Brass"[e]	6×10^{-4}			—
"Cast iron"[e]	3×10^{-4}			—
"Copper"[d]	4×10^{-3}	—	—	—
Annealed copper[i]	2×10^{-3}	—	—	830
Coldworked copper[i]	3×10^{-4}	—	—	650
Tin[c]	7.5×10^{-3}	—	—	—
Lead[c]	1.5×10^{-2}	—	—	75

Figure 12 R values calculated from cutting experiment data in literature and from fracture toughness testing (Atkins, 2003).

Subbiah and Melkote evaluated the Atkins model of machining, which incorporates the energy required for material separation alongside shear and friction energies. The authors conducted orthogonal cutting experiments on oxygen-free high conductivity (OFHC) copper at very low speeds and small uncut chip thicknesses, conditions where the size effect in specific cutting energy is prominent. Scanning electron microscopy (SEM) was used to observe the chip-workpiece interface, providing direct evidence of ductile tearing during material separation (Figure 13), which supports Atkins' hypothesis. By fitting the model to experimental data, the authors found that the fracture toughness and shear yield stress values were of the same order of magnitude as those reported in fracture mechanics studies, validating the model's applicability under conditions with minimal strain rate and temperature effects.

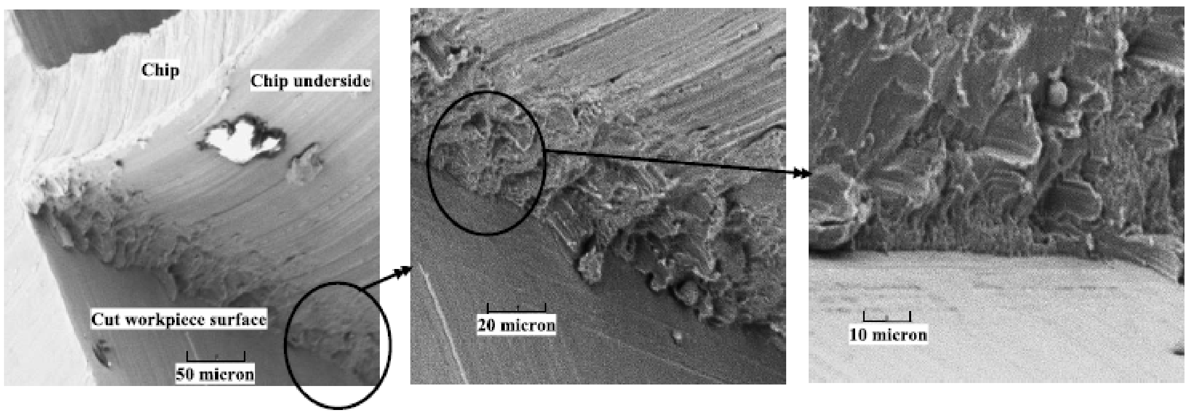

Figure 13 SEM images of chip-workpiece interface (Subbiah & Melkote, 2007).

T.H.C. Childs challenged the claim made by Atkins that ductile fracture energy is a significant contributor to the size effect in metal cutting (Childs, 2010). Atkins had argued that the positive intercept observed in cutting force versus depth plots could be attributed to the energy required to create new surfaces, linking this to material fracture toughness. Childs disputed this view, presenting finite element simulations that showed the size effect can be fully explained by the geometry of the cutting edge and the strain, strain-rate, and temperature dependence of material flow stress.

Childs demonstrated that the cutting edge radius plays a crucial role in influencing forces during chip formation. His simulations showed that the non-zero edge radius leads to "ploughing" forces, which contribute significantly to the observed size effect. By accounting for these forces and the variations in material flow stress with uncut chip thickness, Childs concluded that surface energy contributions are negligible in comparison.

Blackman et al. investigated the role of tool sharpness in machining tests designed to measure fracture toughness (Blackman et al., 2013). The study evaluated whether the fracture toughness values derived from cutting tests are accurate or whether they are dominated by ploughing forces caused by tool bluntness. Cutting experiments were performed on polypropylene (PP) and high-impact polystyrene (HIPS) using tools of varying sharpness, with radii ranging from 5 µm (sharp tools) to 400 µm (blunt tools). A key criterion for distinguishing between sharp and blunt tools was the relationship between the tool tip radius (ρ) and the crack tip opening (δ_c). Tools with $\rho < \delta_c$ were considered sharp, as they directly interacted with the fracture process zone, minimizing ploughing contributions (Figure 14).

The authors demonstrated that cutting with sharp tools provides reliable values that align with conventional fracture toughness measurements, supporting the notion that the cutting process measures a true toughness value independent of ploughing effects. However, when blunt tools are used, the cutting forces include significant contributions from ploughing, which scales linearly with tool tip radius. The study supports Atkins' approach for toughness estimation via cutting but highlights the need to control tool sharpness to ensure valid results.

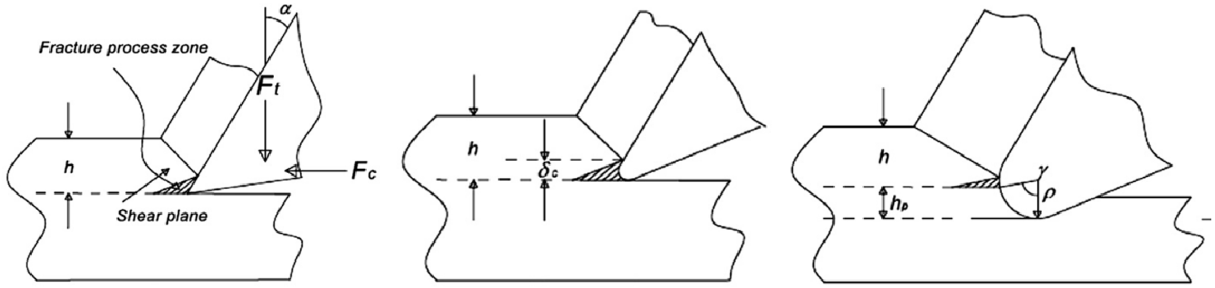

Figure 14 Situations of cutting with different tip radius ρ, left to right: (1) sharp tip; (2) $\rho \leqslant \delta_c$, no ploughing; (3) $\rho \geqslant \delta_c$, ploughing, where δ_c is the critical crack tip opening of the material (Blackman et al., 2013).

Pan et al. investigated the mechanics of material separation in cutting through finite element method (FEM) simulations, using an aluminum alloy as the material of study (Pan et al., 2016). The authors focused on the boundary layers of damage that develop on the underside of the chip and the substrate surface during cutting. Using the Johnson–Cook constitutive and damage models, they simulated continuous chip formation across various uncut chip thicknesses and rake angles. The study reveals that these damage zones, approximately 35 μm thick, remain consistent in size and play a critical role in determining cutting forces and energy dissipation (Figure 15).

This research supports Atkins' model, which incorporates fracture toughness as a critical factor in cutting mechanics. Atkins argued that the work of material separation, rather than surface energy, is essential in explaining cutting behavior and size effects, such as the positive force intercept. Pan et al.'s simulations confirm that the plastic work in the damaged boundary layers contributes to the total work of separation, aligning with Atkins' prediction of uncoupled works of plasticity, friction, and fracture in continuous chip cutting. The study also suggests that it is possible that fracture toughness can be estimated from cutting force data using Atkins' algebraic model (Figure 16). It should be noted that these models utilized a rigid blade and blade tip radius that may crush upon testing due to high stress concentration. Validation testing would be required before it could be said definitively that fracture toughness could be estimated from cutting force.

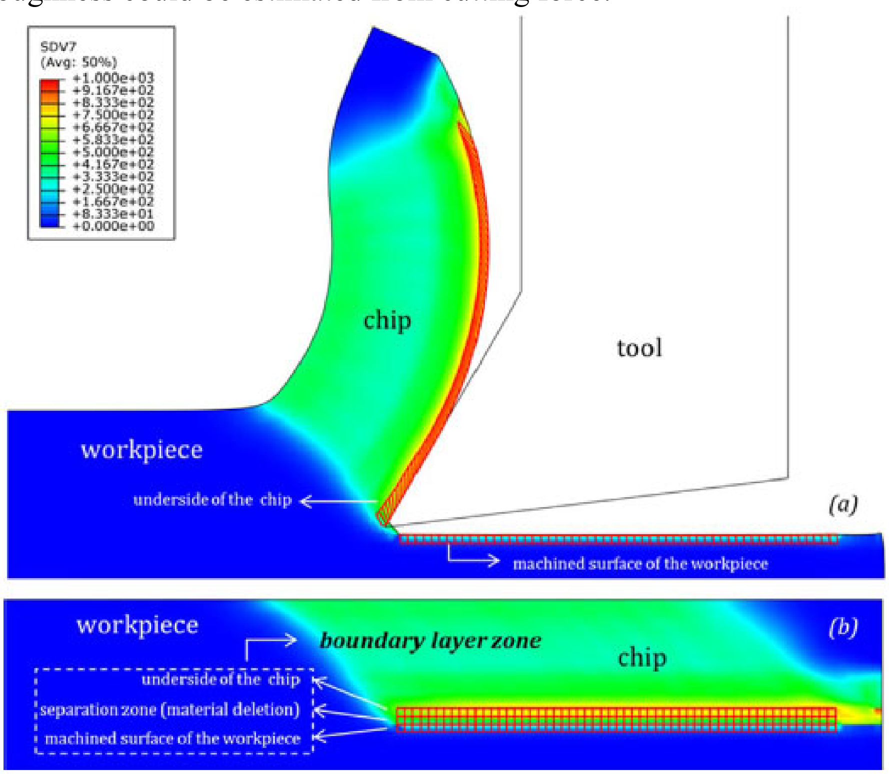

Figure 15 (a) Boundary layer zone on a contour plot of deformed shape. The middle sublayer is invisible due to element deletion; (b) The boundary layer zone contains all three sublayers on the contour plot of undeformed shape (Pan et al., 2016).

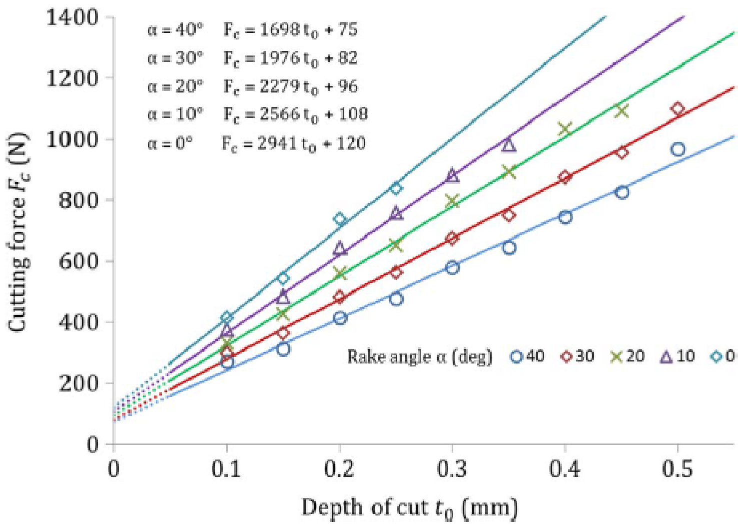

Figure 16 Cutting force versus depth of cut plot and linear curve fitting from finite element simulations (Pan et al., 2016).

3.2 Prediction Models for Pipe Body DBTT

Three prediction models for DBTT in pipeline steel were found in literature and are summarized as follows:

A PRCI report (Dinovitzer et al., 2016) prepared by BMT Fleet Technology explores the development and application of non-destructive techniques to estimate the mechanical properties of vintage pipeline steels, with a focus on predicting Charpy V-notch (CVN) toughness and the ductile-to-brittle transition temperature (DBTT). The project leverages chemical composition, microstructure, and hardness measurements obtained in the field to train a neural network (NN) model for predicting toughness values at selected temperatures. The model was validated through a dataset of 118 vintage pipe materials, encompassing pre-1970s pipelines. A simple engineering software tool, called CheckMate, was developed which allows the user to apply the developed NN algorithm using an MS Excel spreadsheet.

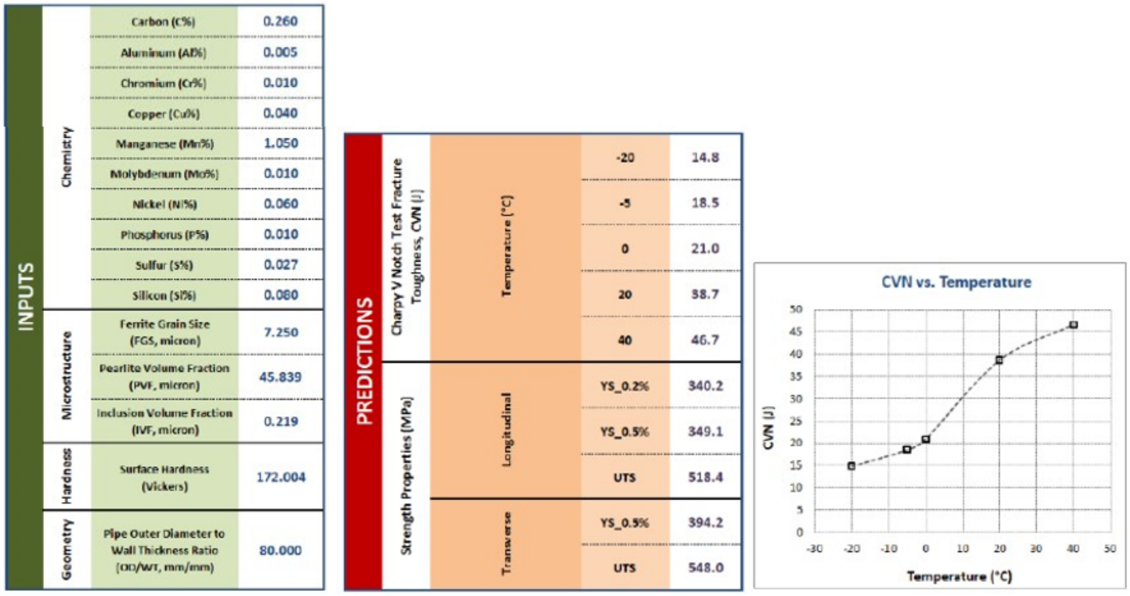

Figure 17 CheckMate spreadsheet inputs and outputs. The model uses 15 parameters and was trained and tested using 118 samples. No blind testing was conducted (Dinovitzer et al., 2016).

Switzner et al. explored the development of predictive models for Charpy V-notch (CVN) toughness and the 85% shear appearance transition temperature (SATT) of steel pipes based on chemical composition and microstructural parameters (Switzner et al., 2021). Using datasets from two vendors, comprising over 8,700 CVN test results and corresponding chemical and microstructural data, the authors built and evaluated both linear regression and random forest models to predict CVN upper shelf energy and SATT. The models indicate strong predictive power, achieving an R^2 value of 0.83 for predicting CVN upper shelf energy and 0.84 for predicting the SATT when simplified to use the four most influential compositional elements: sulfur, silicon, carbon, and manganese.

A subset of the dataset, which included microstructural parameters such as grain size and dark phase (pearlite) fraction, was used to refine the models further. The optimal models for predicting CVN energy and SATT combined microstructural parameters with key compositional elements, achieving R^2 values of 0.87 and 0.77, respectively. Notably, dark phase and manganese emerged as strong predictors for SATT, while sulfur, silicon, and dark phase were most significant for upper shelf energy.

The paper does not explicitly mention other statistical metrics than R^2 value, such as root mean squared error (RMSE), for evaluating the predictive models. The two best results for SATT using (1) random forest model with sulfur, silicon, carbon, and manganese and (2) linear model with manganese, and dark phase are shown in Figure 188 and Figure 199, respectively.

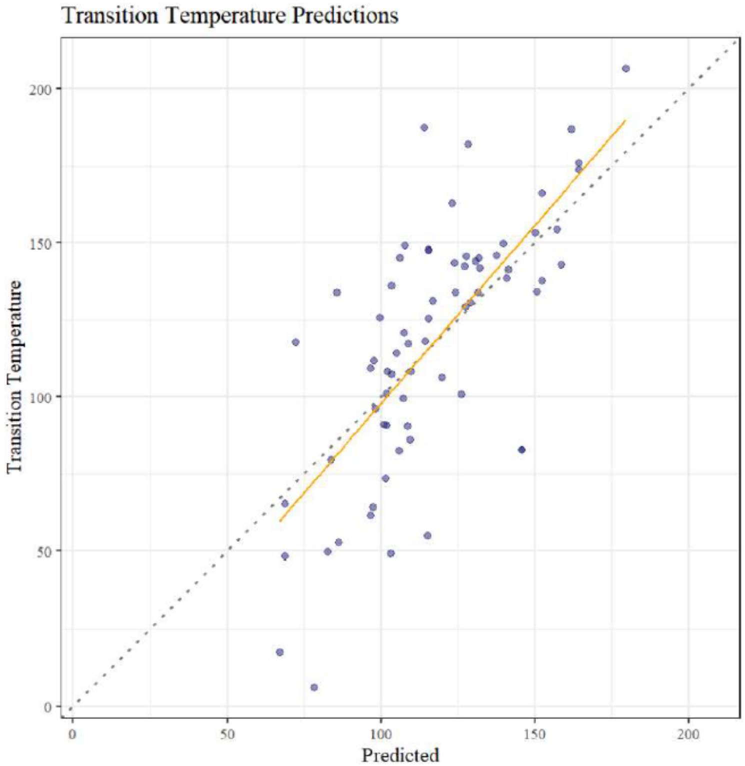

Figure 18 Performance of the random forest model in predicting SATT based on sulfur, silicon, carbon, and manganese content. The model was trained and tested using 398 samples, with 80% allocated for training and 20% for testing. Results displayed are from the test dataset only, and no blind testing was conducted. (Switzner et al., 2021).

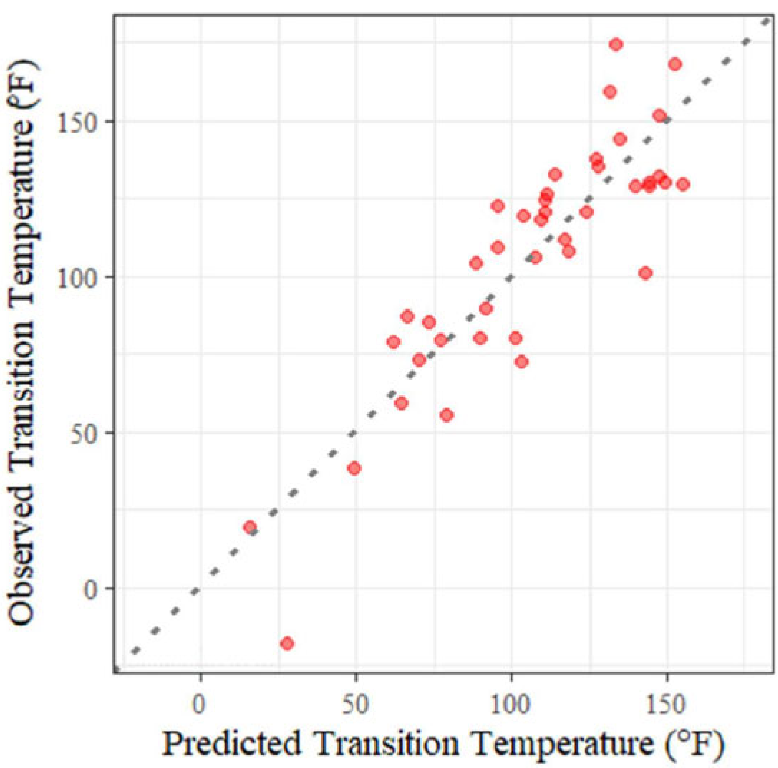

Figure 19 Performance of the linear model in predicting SATT based on manganese and dark phase percentage. The model was fitted using ~50 samples. (Switzner et al., 2021)

Shang et al. explored the use of machine learning (ML) and symbolic regression to predict the ductile-brittle transition temperature (DBTT) of pipeline steel based on chemical composition, mechanical properties, and microstructural characteristics (Shang et al., 2024). The authors assembled a dataset of 36 pipeline steel samples, incorporating information on 11 compositional elements, four mechanical properties, and grain size. Using feature screening techniques, they identified five key factors - carbon (C), silicon (Si), manganese (Mn), tensile strength (TS), and grain size (GS) - as the most influential features affecting DBTT (Figure 2020). Among the eight machine learning models evaluated, the M5P model emerged as the most accurate, achieving R^2 =0.845 and RMSE = 14.65 °C after incorporating the refined feature set (Figure 211). Symbolic regression was used to derive a formula for DBTT:

$$DBTT = -151.66 + 547.36 * C + 201.38 * Si - 18.75 * Mn + 0.07 * TS - 120.11 * GS^{0.5}$$

The study with this formula report an accuracy of R^2 =0.885 in the training data and R^2 =0.857 in the test data. Despite the high correlation it should be noted that this work was not demonstrated experimentally as blind testing was not conducted. Also, a model with 5 inputs developed with only 36 samples suggests that the model could be overfit. Additionally it is not clear which data sets were used for training and validation. Given these highlighted shortcomings, it's possible this is not a direction worth investigating further.

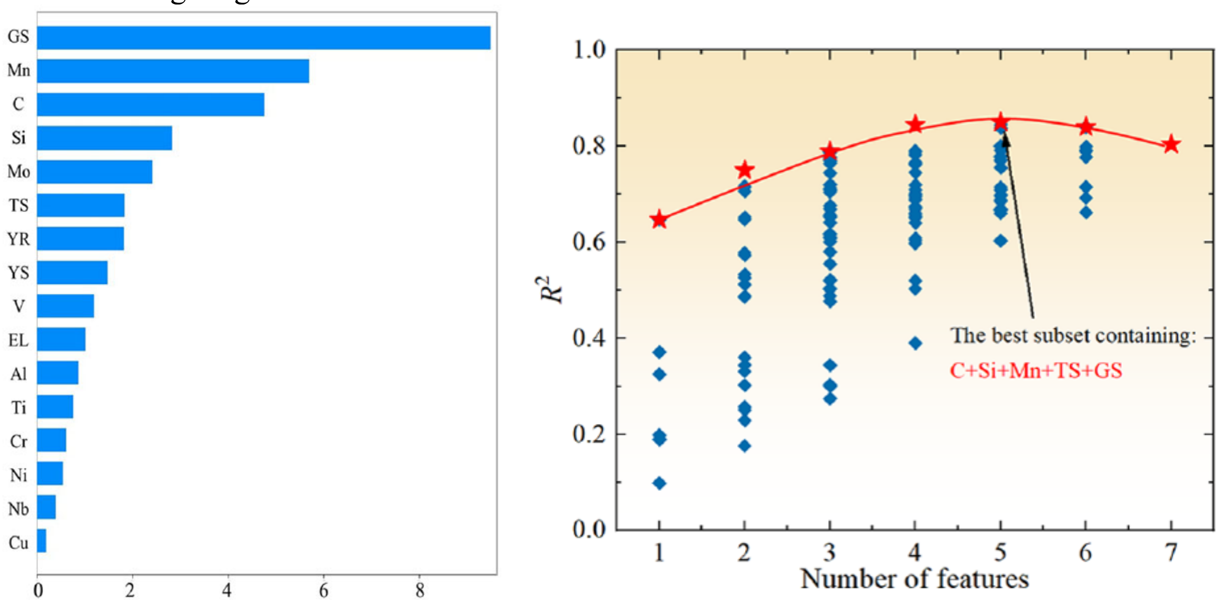

Figure 20 Left: Average impact on model output magnitude from the feature selection process; Right: permutations and combinations of M5P models (Shang et al., 2024).

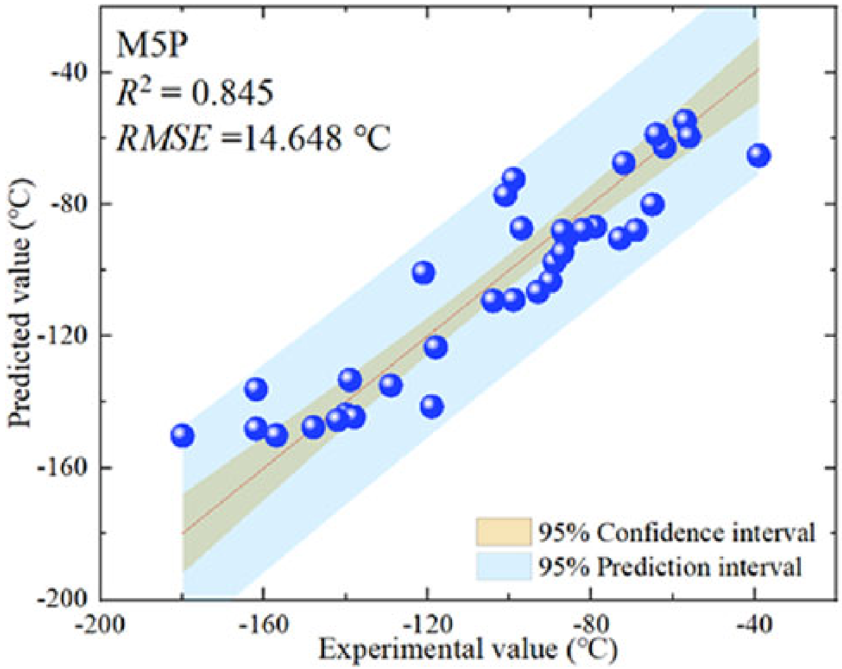

Figure 21 Result of the M5P model using five selected features. The model was trained and tested on 36 samples using ten-fold cross-validation. No blind testing was conducted. (Shang et al., 2024).

3.3 Test Temperature Dependence of Fracture Toughness

The fracture toughness versus temperature curve of metals typically exhibits an exponential increase in the transition region, eventually reaching a plateau at higher temperatures (Figure 22). This behavior reflects the change in dominant fracture mechanisms with temperature. At lower temperatures, fracture occurs through transgranular cleavage, a brittle mechanism characterized by the propagation of cracks along specific crystallographic planes. As the temperature increases, the fracture mechanism transitions to ductile tearing. This process involves the nucleation of microscopic voids at inclusions or second-phase particles, followed by their growth and eventual coalescence, leading to failure. Ductile tearing is associated with higher energy absorption and greater toughness because of the plastic deformation accompanying void formation and growth.

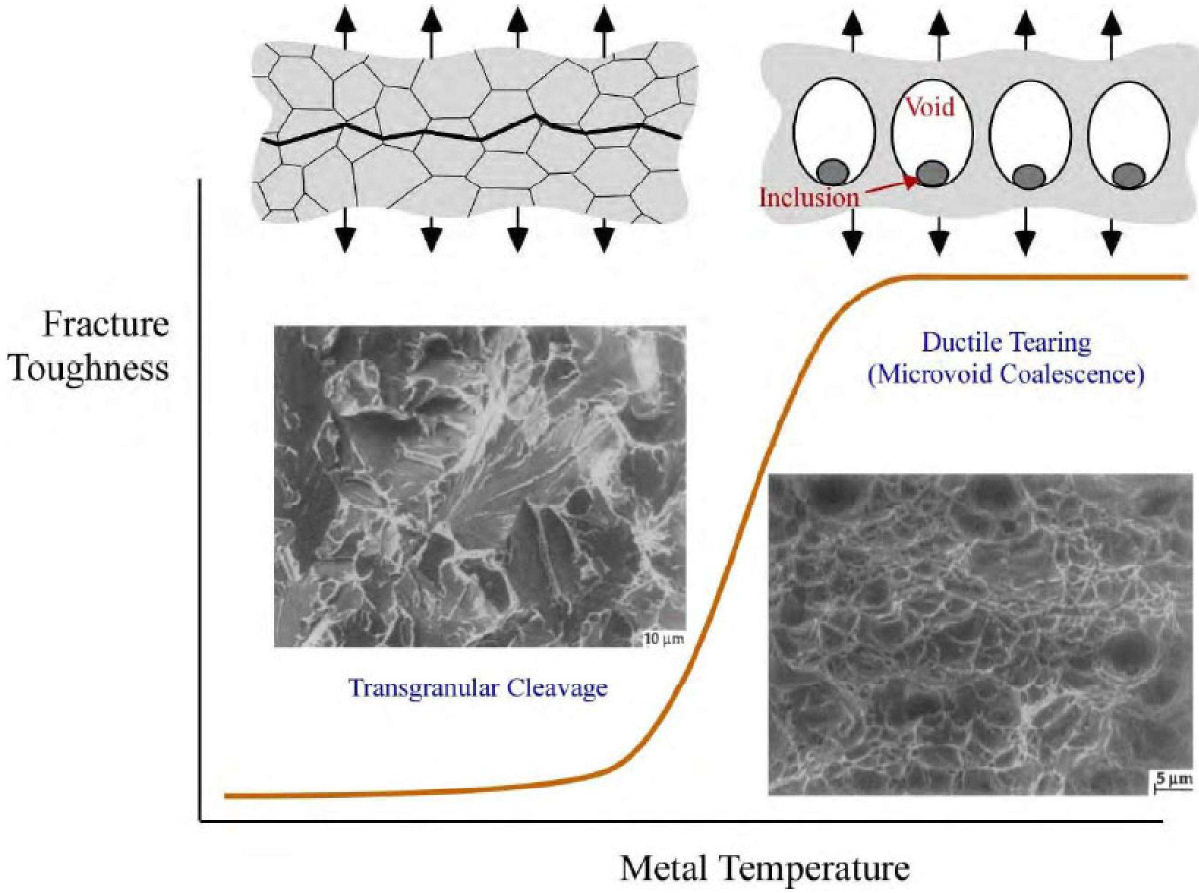

Figure 22 Schematic of fracture toughness versus temperature curve (Anderson, 2023).

According to ASTM E1921 (ASTM International, 2021), the toughness transition curve can be defined using a master curve:

$$K_{Jc\,(median)} = 30 + 70\,exp[0.019(T - T_0)], \qquad MPa\sqrt{m}$$

where $K_{Jc\,(median)}$ is the median value of the elastic-plastic equivalent stress intensity factor derived from the J-integral at the point of onset of cleavage fracture, J_c. T is the test temperature in °C, and T_0 is the reference temperature in °C. The position of the curve on the temperature coordinate is established from the experimental determination of the reference temperature T_0, at which the median K_{Jc} for 1T size specimens is 100 MPa√m (or 91.0 ksi√in).

While T_0 can be determined experimentally following the standard, ASTM E1921 also provides a way to estimate its value using CVN data if a Charpy transition temperature, T_{CVN}, is known corresponding to a 28 J Charpy V-notch energy or a 41 J Charpy V-notch energy:

$$T_0 = T_{CVN} + C$$

where the value C is provided in Table 3 of ASTM E1921-21.

API 579 (American Petroleum Institute, 2016a) provides another equation for estimating T_0:

$$T_0 = T_{CVN,28J} - 77 + \frac{\sigma_{ys}}{12} + \frac{1000}{C_{V-US}}$$

where σ_{ys} is yield stress in MPa, C_{V-US} is the upper shelf CVN energy in J.

Capelle et al. applied the master curve method to evaluate the ductile-brittle transition behavior of API 5L X65 pipeline steel, determining a reference temperature of -128 °C (Capelle et al., 2013). Similarly, Shin et al. applied the master curve method to two API X70 steels and one X80 steel (Shin et al., 2009). They reported reference temperatures of -83 °C and -100 °C for the two X70 steels, and -82 °C for the X80 steel. The variations in among the steels were attributed to differences in microstructure, such as grain size and phase distribution, which influence cleavage fracture resistance. These studies collectively highlight the master curve method as a robust tool for characterizing the fracture toughness of pipeline steels.

In the plateau region, the upper limit of fracture toughness can be determined either through experimental measurements or by estimating it using the yield stress and upper shelf CVN energy, as described by the Rolfe-Novak correlation (Switzner et al., 2024):

$$\left(\frac{K_{limit}}{\sigma_{ys}}\right)^2 = 0.64\left(\frac{C_{V-us}}{\sigma_{ys}} - 0.01\right), \quad (MPa\sqrt{m}, MPa, J)$$

Although the general shape of the fracture toughness versus temperature curve is well understood, converting a K value tested at temperature A to an equivalent value at temperature B requires determining the relative positions of temperatures A and B on the curve (i.e., whether they fall within the transition region or the plateau region). While no specific literature on this topic was identified, some general ideas are provided below:

Idea 1: Compare test temperature with the reference temperature T_0

If the test temperature is significantly above T_0, it is likely in the plateau region. Based on implications from ASTM E1921, a threshold value of 50°C above T_0 could be used.

Idea 2: Identify a K transition temperature (FITT) using CVN test data or SATT prediction models.

Estimate the 85% shear are transition temperature (SATT) from CVN test data or SATT prediction models, and then apply a temperature shift, as outlined in API RP 1176 (American Petroleum Institute, Recommended Practice 1176, 2016), to account for the strain rate difference between CVN testing and quasi-static fracture toughness testing. The temperature shift is calculated as $215 - 1.5 * \sigma_{ys}$. The adjusted fracture initiation transition temperature (FITT) is given by:

$$FITT = SATT - (215 - 1.5 * \sigma_{ys})$$

If the test temperature is higher than FITT, it is in the plateau region; otherwise, it is in the transition region.

Idea 3: Compare K value with the upper shelf estimate.

Compare the measured K value to the estimated upper shelf toughness (e.g., using the Rolfe-Novak correlation). If it is significantly lower, it likely falls in the transition region.

4. Detailed Summary of Key Studies/Findings

4.1.1 Using UT for measuring toughness

Key findings are summarized below:

- **Empirical Correlations Between Ultrasonics and Fracture Toughness**: Many studies demonstrate significant empirical relationships between ultrasonic measurements (attenuation, velocity, and nonlinearity) and fracture toughness. For example, Vary's work illustrates that ultrasonic attenuation correlates strongly with fracture toughness due to underlying microstructural influences such as grain size, dislocation density, and phase morphology. Nonlinear ultrasonic techniques, such as second harmonic generation, have also been shown to effectively estimate fracture toughness in materials like CrMoV rotor steels, correlating the nonlinearity parameter to key fracture parameters.
- **Microstructure's Role in Toughness and Ultrasonics**: Ultrasonic wave interactions are profoundly influenced by material microstructures. Features like grain size, phase distribution, and inclusions govern ultrasonic wave attenuation and velocity, which in turn reflect the material's fracture resistance. In titanium alloys, for example, the alpha-beta phase morphology

is crucial in determining fracture toughness, as verified through both ultrasonic and metallographic analyses (Vary & Hull, 1982).

- **Ultrasonic Testing for Monitoring Material Evolution**: Studies across various alloys reveal consistent trends in ultrasonic properties linked to aging and precipitation hardening. For instance, in aluminum alloys (2024, 7020), sound velocity and electrical conductivity were correlated with impact toughness variations during aging processes, emphasizing the reduction in toughness with peak-aged hardness.

Strengths/Limitations:

Ultrasonic techniques offer rapid, non-destructive, and cost-effective methods for estimating fracture toughness. They are particularly well-suited for in-service monitoring where a single microstructural factor is changing (e.g., aging in aluminum alloys) or for quality assurance/quality control applications (e.g., verifying heat treatments in steels). However, these techniques may be less effective for general fracture toughness measurement across a broad range of materials with diverse microstructures and varying levels of cold working. When multiple microstructural factors change simultaneously, ultrasonic methods may be incapable to differentiate and accurately correlate their individual contributions to toughness. Additionally, interpreting complex microstructural interactions remains challenging. Advancing models to better understand these interactions and bridging empirical observations with theoretical frameworks are critical areas for future development.

4.1.2 Using IIT for measuring toughness

Key findings are summarized below:

- **Methodological Advancements and Key Concepts:** Instrumented indentation techniques have garnered significant attention for estimating fracture toughness, particularly in ductile materials and reactor pressure vessel (RPV) steels. Central to these techniques are models such as the Indentation Energy to Fracture (IEF) and critical stress/strain-based approaches. These methods utilize critical stress, strain, or energy values to determine a critical indentation depth, which is then correlated with the material's fracture toughness. Multiple studies claim that the stress triaxiality beneath the indentation closely resembles the stress field at a crack tip through finite element simulation, supporting the validity of these models.

Strengths/Limitations:

Instrumented indentation offers significant advantages for non-destructive and small-scale evaluations for determining elastic and plastic deformation parameters. Studies for toughness estimations, with a limited sample set and a number of fitting parameter, show correlation with conventional tests (e.g., Lee et al., 2006). Applications extend to localized assessments of welds, heat-affected zones, and thin films, where conventional destructive methods are impractical.

However, instrumented indentation faces fundamental challenges in its methodology. Critics contend that fracture toughness cannot be reliably inferred due to the absence of direct cracking under indentation. Furthermore, the decoupling between tensile properties and fracture toughness undermines the assumption that methods successful in measuring tensile properties can be extended to fracture toughness evaluations (Anderson, 2023).

4.1.3 Using CM for measuring toughness

Key findings are summarized below:

- **Pioneering Insights by Atkins**: Atkins revolutionized the understanding of metal cutting by integrating ductile fracture mechanics into machining models. Unlike traditional analyses that neglected surface work, Atkins demonstrated that the energy required for material separation during cutting is substantial and directly tied to the fracture toughness (R) of the material. His work provided an explanation for phenomena such as size effects and cutting force intercepts, which were previously unexplained by models focusing solely on plasticity and friction.
- **Mechanics of Material Separation**: Subsequent studies validated and expanded Atkins' approach, emphasizing that material separation in cutting is not governed solely by surface energy but by the formation of highly deformed boundary layers adjacent to the cutting plane. These layers, characterized by their toughness-to-strength (R/k) ratio, significantly influence cutting mechanics, including chip formation and cutting forces. Finite Element Method (FEM) simulations confirmed that these damaged layers are a critical factor in separating chips from the workpiece and supported the incorporation of fracture toughness in cutting models.
- **Effect of Tip Radius**: The effect of the cutting tool's tip radius has been extensively studied. A larger tip radius increases the ploughing contribution to cutting forces, which can obscure the true contribution of fracture energy in machining tests. It has been demonstrated that for sharp tools, the energy associated with material separation is dominant and provides a more accurate measure of fracture toughness.

Strengths/Limitations:

Atkins' model has been successfully applied to analyze machining processes across a range of materials, from metals to polymers. For example, machining tests on ductile materials like oxygen-free copper have demonstrated the utility of incorporating material separation energy into cutting models, with results aligning well with experimental observations. However, within the limited materials validated, the estimated values of fracture toughness were generally within the same order of magnitude as those obtained from conventional laboratory testing (e.g., Subbiah & Melkote, 2007). Despite these promising findings, using cutting as a precise and reliable method for measuring fracture toughness has yet to be proven.

4.2 Prediction models for pipe body DBTT

Key findings are summarized below:

- **Advancements in Machine Learning Models**: The prediction of DBTT in pipeline steels has seen significant advancements through the application of machine learning (ML) models. Shang et al. employed a comprehensive dataset encompassing chemical composition, mechanical properties, and grain size characteristics to develop predictive models. Using techniques like symbolic regression and various ML algorithms (e.g., Random Forest, K-Nearest Neighbors), the models achieved high accuracy in predicting DBTT, with the M5P algorithm demonstrating the best performance ($R^2 = 0.822$, RMSE = 14.66°C). These models have been instrumental in identifying key features affecting DBTT, such as grain size, carbon content, and yield strength.
- **Integration of Chemical Composition and Microstructure**: Studies by Switzner et al. emphasized the role of chemical composition and microstructure in determining pipeline steel toughness. By analyzing data from over 1,500 pipe samples, relationships between DBTT and elements like manganese, carbon, and sulfur were established. Refining grain size and

minimizing inclusions were found to lower the DBTT, highlighting the importance of microstructural optimization in steel processing. The proposed models successfully linked non-destructive composition and metallographic data with Charpy V-notch test results.

Strengths/Limitations:

While these studies have successfully identified critical parameters influencing fracture toughness and achieved high coefficients of determination (R^2) in their models, there are notable limitations that need to be addressed. Firstly, none of the studies conducted blind testing to validate the performance of their predictive models against unseen data. This lack of independent validation makes it challenging to accurately evaluate the true predictive accuracy and reliability of these models when applied to new or untested pipeline materials.

Additionally, in the case of Shang's model, there are concerns about potential overfitting. The model uses five parameters to predict the ductile-brittle transition temperature (DBTT) but is based on a relatively small dataset of only 36 samples.

4.3 Test temperature dependence of K value

Key findings are summarized below:

- **Fracture Toughness versus Temperature Curve**: The relationship between fracture toughness and test temperature generally follows an exponential trend in the transition region, which can be effectively described using a master curve for ferritic steels. At higher temperatures, the curve levels off into a plateau, where the limiting value can be estimated using the upper-shelf CVN value and the Rolfe-Novak correlation. The reference temperature in the master curve can be estimated using equations provided in ASTM E1921 or API 579.

5. Synthesis and Interpretation

5.1 Microstructural factors influencing fracture toughness

Research across various studies has consistently highlighted the critical role of microstructure in determining material fracture toughness, with grain size emerging as a particularly influential factor (e.g., Shang et al., 2024; Vary, 1979). Grain size significantly affects fracture mechanics by influencing crack propagation and the energy required for fracture initiation. Smaller grain sizes typically enhance toughness by increasing the number of grain boundaries, which absorb and deflect crack energy, impeding crack propagation. In addition to improving cleavage resistance, grain refinement lowers the ductile-to-brittle transition temperature (DBTT), enabling materials to remain ductile at lower temperatures. The relationship between grain size and toughness is often described by the Hall-Petch relation, which predicts that properties such as cleavage fracture stress and DBTT vary inversely with the square root of grain size (Morris Jr, 2001; Rosenfield et al., 1972).

Beyond grain size, other microstructural features, such as the volume fraction of pearlite, have been identified as significant factors influencing fracture toughness, have been identified as influential factors in fracture toughness. Studies (Dinovitzer et al., 2016; Switzner et al., 2024) have observed that pearlite, often referred to as the "dark phase" in steel microstructures, can substantially affect toughness. Higher pearlite content, with its harder and more brittle nature compared to ferrite, tends to reduce fracture toughness (Rosenfield et al., 1972)

5.2 Surface-to-bulk property correction

Ersoy et al. investigated the differences between surface and bulk properties (e.g., chemistry, grain size, yield, and tensile strength) in a GTI report to PHMSA (Ersoy et al., 2021). The report identified three primary factors contributing to these differences: (a) cold work and forming stress introduced during pipe manufacturing, (b) chemical segregation from primary steel production processes (e.g., rimmed/capped centerline carbon segregation), and (c) grain refinement in high-strength low-alloy (HSLA) steels, particularly near the outer surfaces of the pipe wall.

It is postulated that fracture toughness in pipes exhibits similar surface-to-bulk differences, as the factors mentioned above can also influence material toughness. However, this surface-to-bulk correction is rarely addressed in the literature concerning surface measurement methods (e.g., Instrumented Indentation Testing (IIT) and Charpy Measurement (CM)) or ductile-to-brittle transition temperature (DBTT) prediction models. One exception is the neural network model developed by Dinovitzer et al., where the pipe outer diameter-to-wall thickness ratio was included as an input parameter. This accounted for the work hardening effects induced by forming and expansion processes, particularly in seam-welded pipes (Dinovitzer et al., 2016).

5.3 Cutting tool radius

As summarized in Section 4.1.3, the effect of cutting tool radius has been extensively discussed in the literature on using cutting methods to measure fracture toughness. While the underlying mechanism differs for the BTM technology, the cutting tool radius is still critical, as it influences the initial deformation of the material flowing into the stretch passage.

Building on these findings, we have developed a plan to test blades with varying tip radii as part of Task 1.3. This will help determine the optimal blade geometry for achieving accurate and reliable fracture toughness measurements with the BTM technology.

6. Identification of Gaps

6.1 State-of-the-art NDE methods for measuring fracture toughness

This report reviews three existing NDE methods for measuring fracture toughness: Ultrasonic Testing (UT), Instrumented Indentation Testing (IIT), and Cutting. While each method has achieved varying degrees of success, none has reached the level of accuracy or versatility necessary for widespread commercial application. The literature reveals that none of these methods has been validated through blind testing with a large sample set (e.g., more than 30 different steels). Furthermore, no field device has been developed for UT or Cutting to measure fracture toughness, to the best of the author's knowledge. Although IIT has a field tool (Haggag, 2007), the lack of a fundamental link between indentation mechanics and fracture toughness undermines the reliability of the technology. Among the different prior techniques surveyed, only cutting includes measuring the material response to an actual material separation to evaluate the cracking resistance.

6.2 Prediction models for pipe DBTT

Three prediction models for pipe steel ductile-brittle transition temperature were found in literature, two of them do not give statistics except for R^2 values, which makes it hard to evaluate their prediction accuracy. The model by Zhang et al. does give the root mean square error (RMSE) of 14.65 °C for their best model.

MMT has developed an internal machine learning model for DBTT predictions. The model is trained and validated using 60 and 27 samples, respectively. The unity plot comparing the predicted DBTT and lab measured DBTT (from fitting CVN data at multiple temperatures) is given in Figure 23. The RMSE for all samples is 11.4 °C, which outperforms the model in Zhang's paper. However, the model was likely overfit based on the number of fitting parameters and the absence of blind testing.

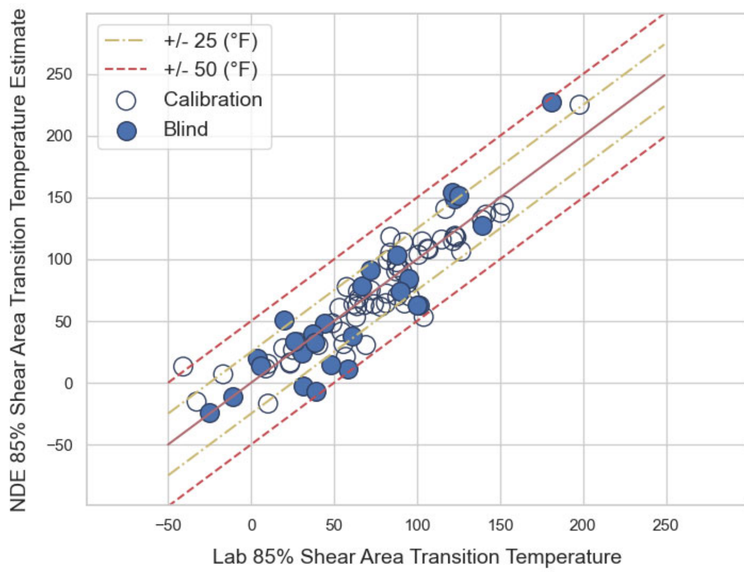

Figure 23 Unity plot of prediction DBTT versus lab DBTT from internal MMT model.

A review of our internal database also revealed a simple criterion for identifying pipes with a high Fracture Initiation Transition Temperature (FITT): a grain size exceeding 25 µm. Applying this criterion excludes 5 samples out of the 106 in the database, 2 of which has a FITT exceeding 55 °F, which is the assumed operating temperature (Figure 24).

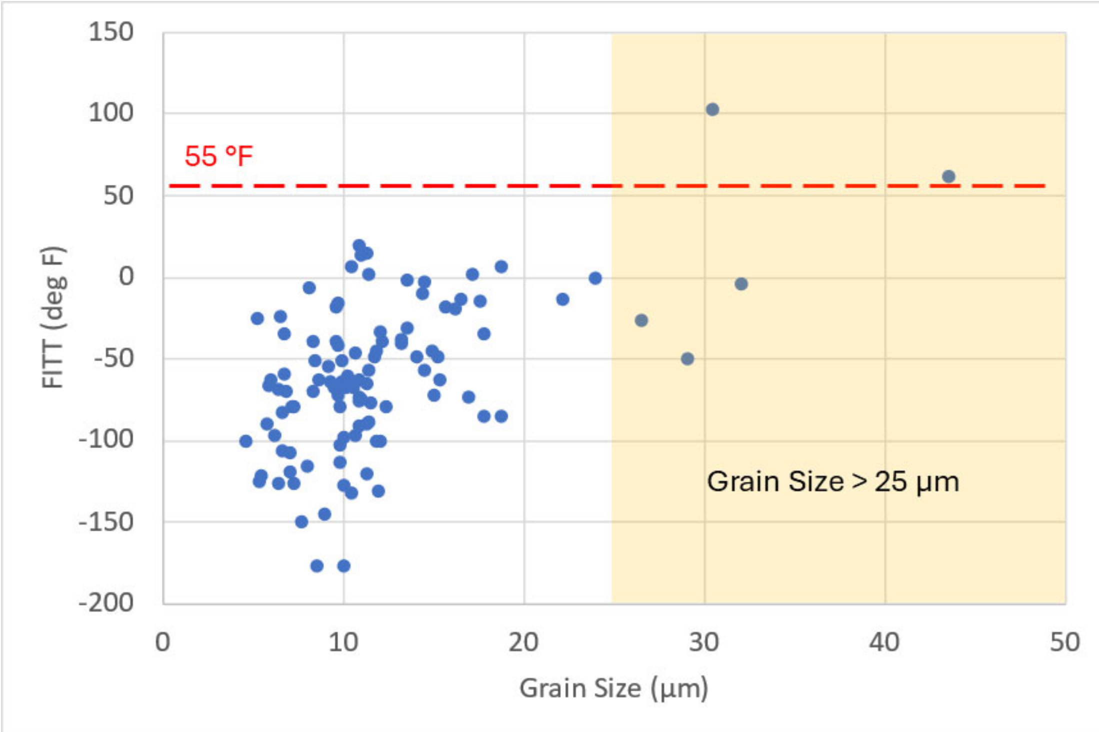

Figure 24 FITT versus grain size from MMT internal database.

6.3 Test temperature dependence of K value

Although the general shape of the fracture toughness versus temperature curve is well understood, determining whether a given test temperature falls within the transition region or the plateau region remains challenging. If the transition temperature for a sample could be approximately estimated either from CVN test data or from a SATT prediction model, we could flag samples with test temperatures near this transition (based on the accuracy of the estimation) and consider excluding them from model development until further analysis or testing can be conducted. We will continue to investigate this issue and seek input from the TAP members to refine our approach.

7. Conclusion

7.1 State-of-the-art NDE methods for measuring fracture toughness

The literature review examines three primary non-destructive testing (NDT) methods for measuring fracture toughness—Ultrasonic Testing, Instrumented Indentation, and Cutting. While each method has achieved varying degrees of success, none has reached the level of accuracy or versatility required for widespread commercial application. The review outlines the advantages and limitations of each approach.

In comparison to these existing technologies, the Blade Toughness Meter (BTM) offers a significant advantage by introducing a controlled microcrack into the material, leaving fracture surfaces on the ligaments of the substrate and the chip underside. The characteristics of these ligaments, including their fracture surfaces, exhibit a direct correlation with material fracture toughness. This correlation will be further explored in an upcoming PPIM paper.

Over the past decades, numerous attempts have been made to relate material fracture toughness to responses from surface testing. However, studies applying these methods to steel systems often lack sufficient validation testing to verify whether the observed performance would hold under blind testing. Blind testing refers to a validation process where a model or method is tested on a completely unseen dataset, ensuring that the results are not influenced by prior knowledge of the data or any biases introduced during model development. This rigorous approach evaluates the true predictive capability and generalizability of a method. This project aims to address this gap through extensive blind testing of the BTM technology. Approximately 100 pipes with a range of fracture toughness values will undergo lab testing to train, validate, and blind-test the developed model. Without such validation approach, there is a greater risk of over fitting with more complex models or more parameters than what is optimal for testing unknown samples.

7.2 Prediction models for pipe DBTT

Three prediction models for the ductile-to-brittle transition temperature (DBTT) of steel pipes were identified in the literature and reviewed. While these models generally report high coefficients of determination (R^2) when compared to lab-measured values, none have undergone blind testing to validate their performance on unseen data. Consequently, the accuracy of these models remains uncertain, and their application in the field is limited, as no conservative shift can be calculated and applied.

7.3 Test temperature dependence of K value

Normalizing the temperature dependence of K test values remains a challenge, as evidenced by a review of related ASTM and API standards. Methods to identify whether a test temperature falls within the transition region or plateau region require further investigation. Preliminary ideas proposed in Section 3.3 will be solidified and tested as part of this project (also included in Task 2.2). We will continue to explore this issue and seek input from TAP members to enhance our approach and ensure robust solutions.

References

American Petroleum Institute. (2016a). *API 579-1/ASME FFS-1: Fitness-for-Service*.

American Petroleum Institute. (2016b). *API RP 1176: Recommended Practice for Assessment and Management of Cracking in Pipelines*.

Anderson, T. (2023). Measuring Toughness with Instrumented Indentation Methods: Fact or Fiction? *35th International Pipeline Pigging and Integrity Management Conference (PPIM 2023)*, 1023–1036. https://doi.org/10.52202/068696-0064

ASTM International. (2021). *Test Method for Determination of Reference Temperature, To, for Ferritic Steels in the Transition Range*. ASTM International. https://doi.org/10.1520/E1921-21A

Atkins, A. G. (2003). Modelling metal cutting using modern ductile fracture mechanics: Quantitative explanations for some longstanding problems. *International Journal of Mechanical Sciences*, *45*(2), 373–396. https://doi.org/10.1016/S0020-7403(03)00040-7

Blackman, B. R. K., Hoult, T. R., Patel, Y., & Williams, J. G. (2013). Tool sharpness as a factor in machining tests to determine toughness. *Engineering Fracture Mechanics*, *101*, 47–58. https://doi.org/10.1016/j.engfracmech.2012.09.020

Byun, T. S., Kim, J. W., & Hong, J. H. (1998). A theoretical model for determination of fracture toughness of reactor pressure vessel steels in the transition region from automated ball indentation test. *Journal of Nuclear Materials*, *252*(3), 187–194.

Byun, T. S., Kim, S. H., Lee, B. S., Kim, I. S., & Hong, J. H. (2000). Estimation of fracture toughness transition curves of RPV steels from ball indentation and tensile test data. *Journal of Nuclear Materials*, *277*(2–3), 263–273. https://doi.org/10.1016/S0022-3115(99)00197-X

Capelle, J., Furtado, J., Azari, Z., Jallais, S., & Pluvinage, G. (2013). Design based on ductile–brittle transition temperature for API 5L X65 steel used for dense CO2 transport. *Engineering Fracture Mechanics*, *110*, 270–280. https://doi.org/10.1016/j.engfracmech.2013.08.009

Childs, T. H. C. (2010). Surface energy, cutting edge radius and material flow stress size effects in continuous chip formation of metals. *CIRP Journal of Manufacturing Science and Technology*, *3*(1), 27–39. https://doi.org/10.1016/j.cirpj.2010.07.008

Dinovitzer, A., Ghovanlou, M., & (Archived), N. P. (2016). *PR-214-123734-R01 In The Ditch Non-Destructive Mechanical Property Measurement* (No. Pages 76; p. Pages 76). Pipeline Research Council International, Inc. (PRCI). https://doi.org/10.55274/R0011019

Ersoy, D., Miller, B., Merino, M. G., Liu, Y., Zhang, Q., Chen, J., & Xu, N. (2021). Validating non-destructive tools for surface to bulk correlations of yield strength, toughness, and chemistry. *GTI Project*, *22428/22429*.

Gür, C. H., & Yildiz, I. (2008). Utilization of Non-destructive Methods for Determining the Effect of Age-Hardening on Impact Toughness of 2024 Al–Cu–Mg Alloy. *Journal of Nondestructive Evaluation*, *27*(4), 99–104. https://doi.org/10.1007/s10921-008-0028-2

Gür, C. H., & Yıldız, İ. (2004). Non-destructive investigation on the effect of precipitation hardening on impact toughness of 7020 Al–Zn–Mg alloy. *Materials Science and Engineering: A*, *382*(1–2), 395–400.

Haggag, F. M. (2007). Innovative SSM technology determines structural integrity of metallic structures: Example applications for pressure vessels and oil and gas pipelines. *International Journal of Pure and Applied Physics*, *3*(1), 91–108.

Haggag, F. M., Byun, T.-S., Hong, J. H., Miraglia, P. Q., & Murty, K. L. (1998). Indentation-energy-to-fracture (IEF) parameter for characterization of DBTT in carbon steels using nondestructive automated ball indentation (ABI) technique. *Scripta Materialia*, *38*(4), 645–652.

Haggag, F. M., & Nanstad, R. K. (1989). *Estimating fracture toughness using tension or ball indentation tests and a modified critical strain model*. Oak Ridge National Lab.(ORNL), Oak Ridge, TN (United States).

Huang, X., Feigel, B., Ryan, A., Rizwan I Haque, I., Willey, B., & Bellemare, S. C. (2024). In-Situ Determination of Pipe Body Fracture Toughness Using Planing-Induced Microfracture Method. *Volume 2A: Pipeline and Facilities Integrity*, V02AT03A034. https://doi.org/10.1115/IPC2024-133317

Jeon, S.-W., Lee, K.-W., Kim, J. Y., Kim, W. J., Park, C.-P., & Kwon, D. (2017). Estimation of fracture toughness of metallic materials using instrumented indentation: Critical indentation stress and strain model. *Experimental Mechanics*, *57*, 1013–1025.

Jeong, H., Nahm, S.-H., Jhang, K.-Y., & Nam, Y.-H. (2003). A nondestructive method for estimation of the fracture toughness of CrMoV rotor steels based on ultrasonic nonlinearity. *Ultrasonics*, *41*(7), 543–549.

Krüger, S. E., Rebello, J. M. A., & De Camargo, P. C. (1999). Hydrogen damage detection by ultrasonic spectral analysis. *Ndt & E International*, *32*(5), 275–281.

Lee, J.-S., Jang, J., Lee, B.-W., Choi, Y., Lee, S. G., & Kwon, D. (2006). An instrumented indentation technique for estimating fracture toughness of ductile materials: A critical indentation energy model based on continuum damage mechanics. *Acta Materialia*, *54*(4), 1101–1109.

Morris Jr, J. W. (2001). *The influence of grain size on the mechanical properties of steel*.

Pan, H., Liu, J., Choi, Y., Xu, C., Bai, Y., & Atkins, T. (2016). Zones of material separation in simulations of cutting. *International Journal of Mechanical Sciences*, *115–116*, 262–279. https://doi.org/10.1016/j.ijmecsci.2016.06.019

Rosenfield, A. R., Hahn, G. T., & Embury, J. D. (1972). Fracture of steels containing pearlite. *Metallurgical Transactions*, *3*(11), 2797–2804. https://doi.org/10.1007/BF02652845

Shang, C., Zhu, D., Wu, H.-H., Bai, P., Hou, F., Li, J., Wang, S., Wu, G., Gao, J., Zhou, X., Lookman, T., & Mao, X. (2024). A quantitative relation for the ductile-brittle transition temperature in pipeline steel. *Scripta Materialia*, *244*, 116023. https://doi.org/10.1016/j.scriptamat.2024.116023

Shin, S. Y., Woo, K. J., Hwang, B., Kim, S., & Lee, S. (2009). Fracture-Toughness Analysis in Transition-Temperature Region of Three American Petroleum Institute X70 and X80 Pipeline Steels. *Metallurgical and Materials Transactions A*, *40*(4), 867–876. https://doi.org/10.1007/s11661-008-9764-2

Smith, R. L., & Reynolds, W. N. (1982). The correlation of ultrasonic attenuation, microstructure and ductile to brittle transition temperature in very low carbon steels. *Journal of Materials Science*, *17*(5), 1420–1426. https://doi.org/10.1007/BF00752255

Subbiah, S., & Melkote, S. N. (2007). Evaluation of Atkins' model of ductile machining including the material separation component. *Journal of Materials Processing Technology*, *182*(1–3), 398–404. https://doi.org/10.1016/j.jmatprotec.2006.08.019

Switzner, N., Anderson, J., Martin, P., Lanya Ahmed, & Veloo, P. (2024). *Estimating Fracture Toughness for Pipeline Steel from Charpy V-Notch Data using the API-579 Master Curve Method*. https://doi.org/10.13140/RG.2.2.12810.27843

Switzner, N., Anderson, J., Rosenfeld, M., Gibbs, J., Veloo, P., & Gonzalez, R. (2021). Assessing steel pipe toughness using chemical composition and microstructure. *Pipeline Pigging and Integrity Management (PPIM) Conference, Houston, TX, USA*.

Vary, A. (1978). *CORRELATIONS AMONG ULTRASONIC PROPAGATION FACTORS AND FRACTURE TOUGHNESS PROPERTIES OF METALLIC MATERIALS.*

Vary, A. (1979). Correlations Between Ultrasonic and Fracture Toughness Factors in Metallic Materials. In C. Smith (Ed.), *Fracture Mechanics* (pp. 563-563–16). ASTM International. https://doi.org/10.1520/STP34936S

Vary, A. (1982). Fundamentals of ultrasonic NDE for microstructure/material property interrelations. *Advanced Materials Technology*.

Vary, A. (1989). Concepts for interrelating ultrasonic attenuation, microstructure, and fracture toughness in polycrystalline solids. *NDT International*, *22*(5), 306. https://doi.org/10.1016/0308-9126(89)91482-X

Vary, A., & Hull, D. R. (1982). Interrelation of material microstructure, ultrasonic factors, and fracture toughness of two phase titanium alloy. *Spring Conf. of the Am. Soc. for Nondestructive Testing*, *E-1151*.

Williams, C., Borigo, C., Rivière, J., Lissenden, C. J., & Shokouhi, P. (2022). Nondestructive Evaluation of Fracture Toughness in 4130 Steel Using Nonlinear Ultrasonic Testing. *Journal of Nondestructive Evaluation*, *41*(1), 13. https://doi.org/10.1007/s10921-022-00846-5

Attachment 2 – Task 1.2 – BTM Finite Element Model Development Progress Report

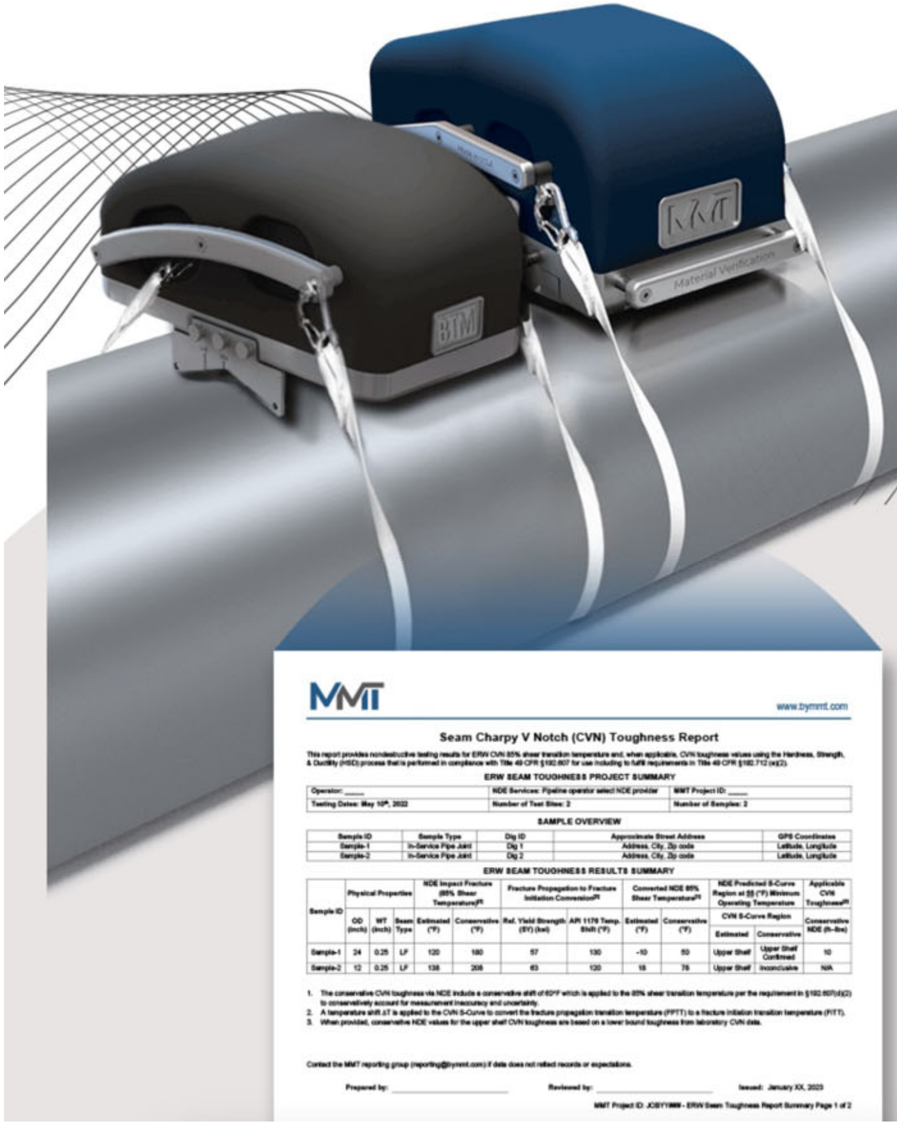

MMT

R&D Project:
Development of the Blade Toughness Meter (BTM) for In -Situ Pipe Toughness Measurement

Co-sponsored By PHMSA
(Project # 1043)

Milestone 1.2 – Progress Report
01/15/2025

Milestone 1.2 Finite Element Model Development (Physical modeling)

Proposal: MMT plans to develop an FE model internally or with external academic partners to understand better the science behind the planing-induced fracture method, including the stress-strain state of the material within the stretch passage and the stress on the cutting blade. The FE model, a simulation of a real -life BTM test, will utilize material models with a wide range of strength and toughness properties, allowing geometric characteristics of the pipeline ligaments measured in the field to be better related to their toughness properties.

This report (Reached 25% of milestone completion on MMT work):

- 1.2.1: Retrieve and re-interpret prior FEA work done by MMT
- 1.2.2: Detailed review and insight from prior FEA work by Bai et al. and select physical experiments
- 1.2.3: First tangible outcome: Initial physical modeling completed
- 1.2.4: Ongoing: Additional review of material response during tests (Significant effort added to the initial plan)
- 1.2.5: Next step: 3D simulation without stretch passage

Task 1.2.1 (1/2): Retrieve and re -interpret prior FEA work done by MMT

- Prior work completed: 3D proof of concept of simulation in the stretch passage (Details on page 2/2)
  (Pivoted to 2D simulation to optimize the cutting edge - Not critical to Milestone 1.2 by itself)

- Finding: Able to successfully simulate deformation and capture the accumulated damage (<u>It can be done</u>)

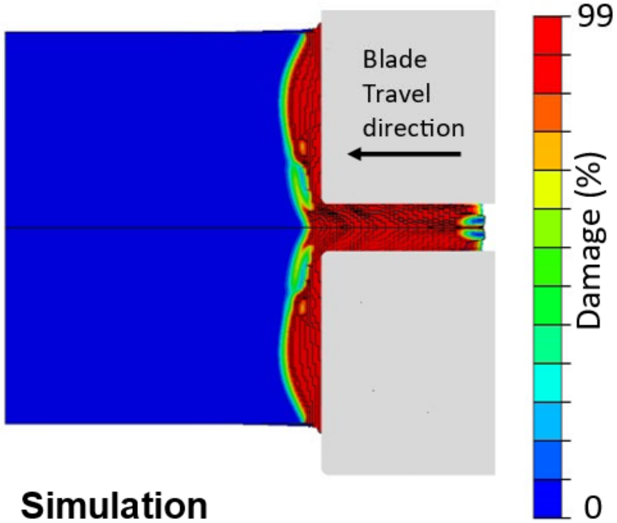

Simulation
(Shown in cutting plane)

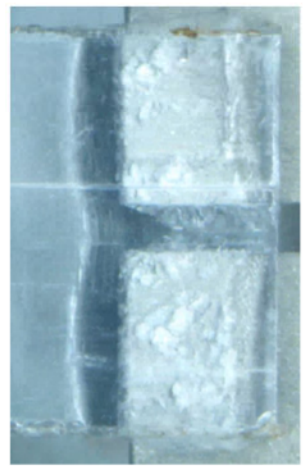

Experiment
(Polycarbonate)

Limitations:
- Actual element deletion was going to be the next step
- Only one material condition was tested (one set of plasticity parameters and nominal values for the damage model)
- Slow (runtime 2 days)

Task 1.2.1 (2/2) : Retrieve and re -interpret prior FEA work done by MMT

- Prior FEA work utilized coupled Eulerian -Lagrangian simulations
  - Multilinear Isotropic Hardening Plasticity Model with Bao -Wierzbicki failure framework
- Model validated on side by side of simulated and actual lab results for tensile test & CT test
  - Good agreement in tensile test (**Fig. 1**)
  - Okay agreement in CT test (**Fig. 2**)
    - Also saw agreement in shape of stress/strain fields
- Same model parameters utilized for 3d simulation of BTM test (**Fig 3.**) (**Fig 4.**)

$$\sigma = \sigma_y \left(1 + \frac{E}{\sigma_y}\varepsilon_p\right)^n$$

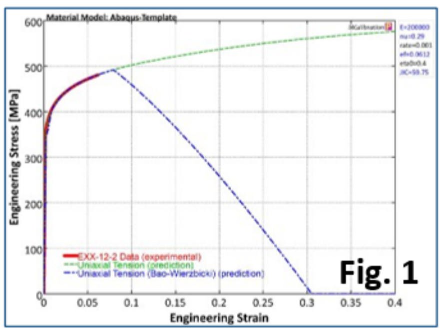

Fig. 1

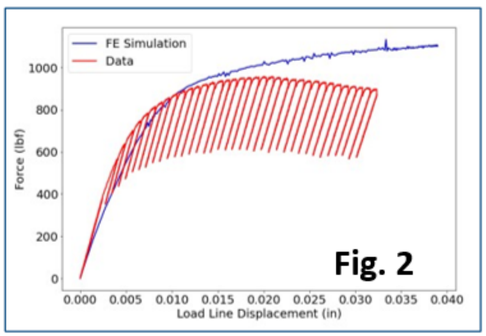

Fig. 2

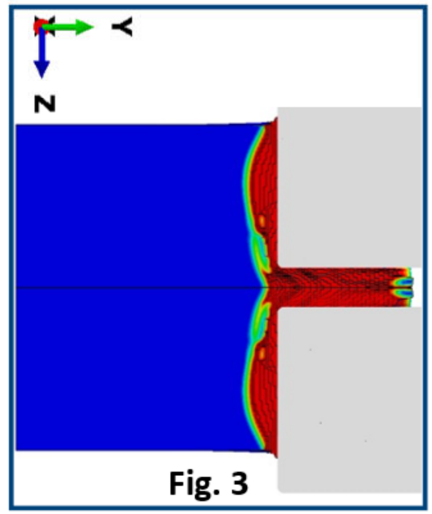

Fig. 3

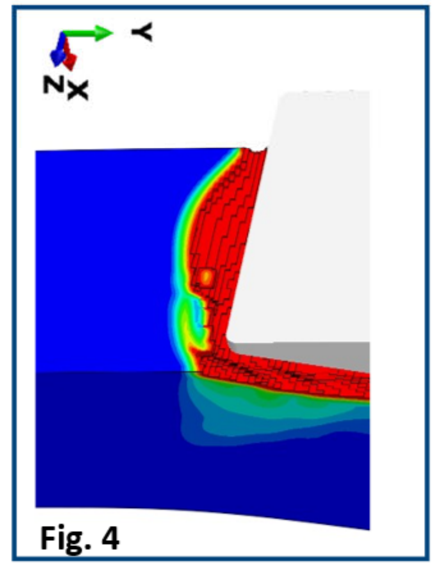

Fig. 4

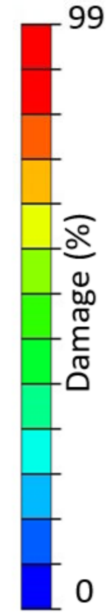

Task 1.2.2 (1/3) : Prior FEA work – Bai *et al.*

- A thermomechanical 2D plane strain model in Abaqus Explicit. Rigid tool body with sharp tip.
- The Johnson-Cook plasticity and damage models are used. Elements are deleted when the damage indicator exceeds unity.
- The model predicted formation of continuous chip at larger rake angle and smaller depth of cut. This is consistent with MMT observations from the previous NDTT and current BTM experiments.

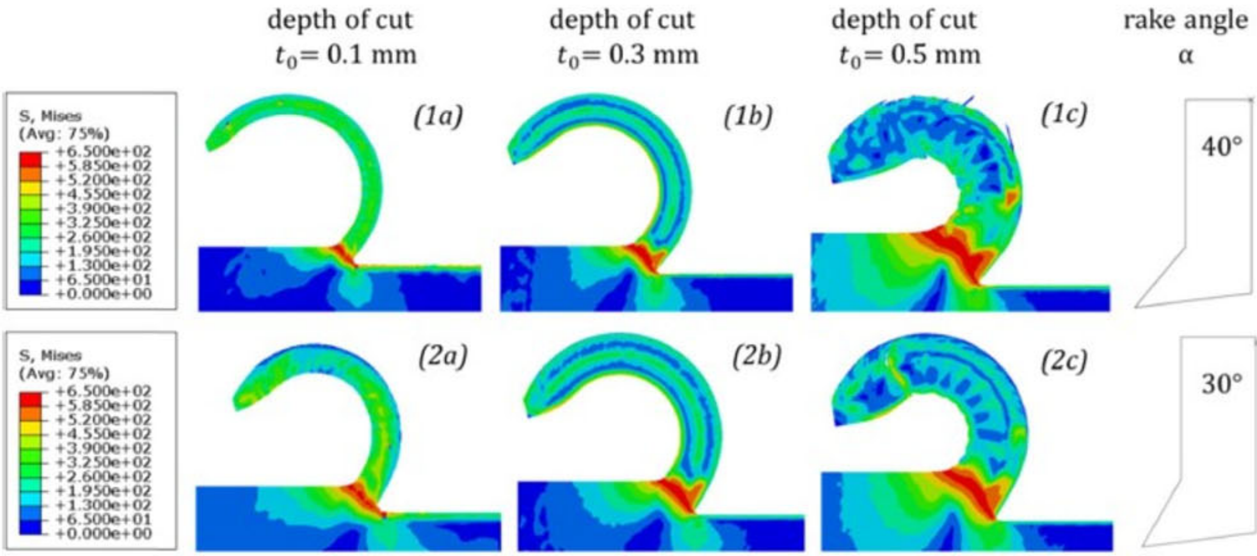

Task 1.2.2 (2/3) : Preliminary FEA work for MMT – Bai

Recent 2-D simulations on tip radius effect.
(Color represents equivalent plastic strain)

Top Row: Sharp tip

Bottom Row: Tip radius of 0.02mm

Adding a tip radius results in rougher cut surface and an elevated cutting force.

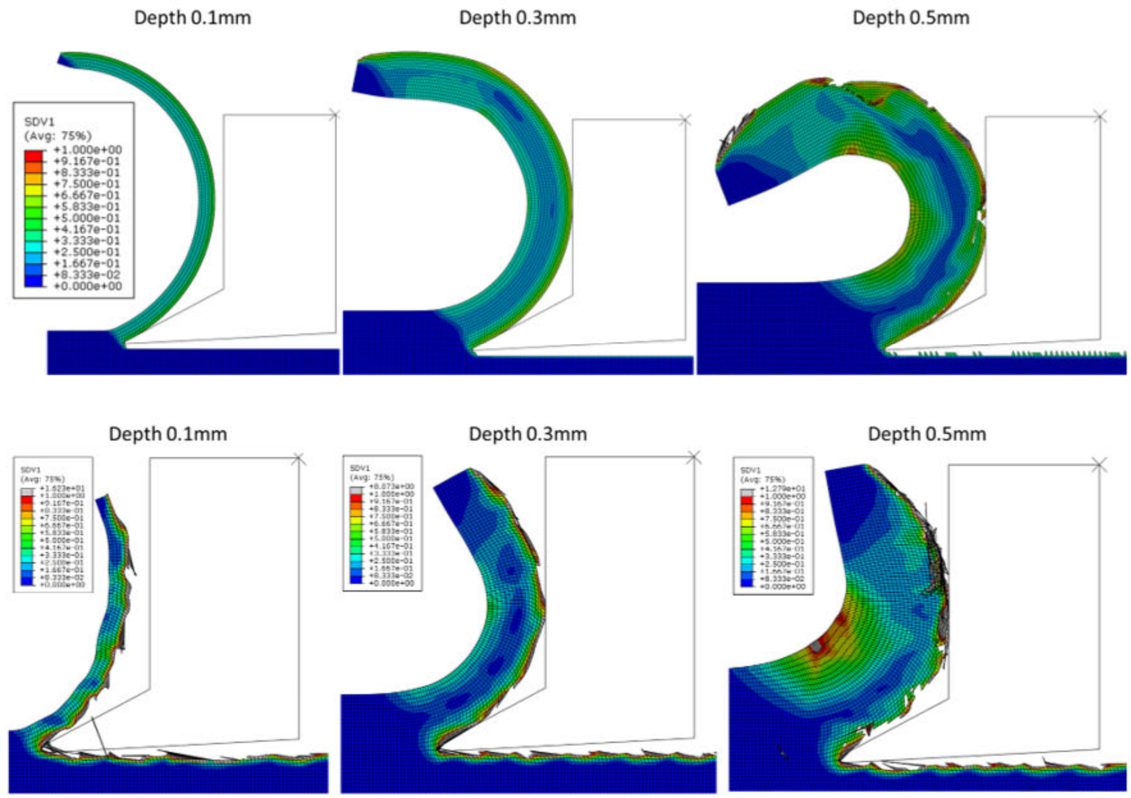

Add-On: Insight from Experiments

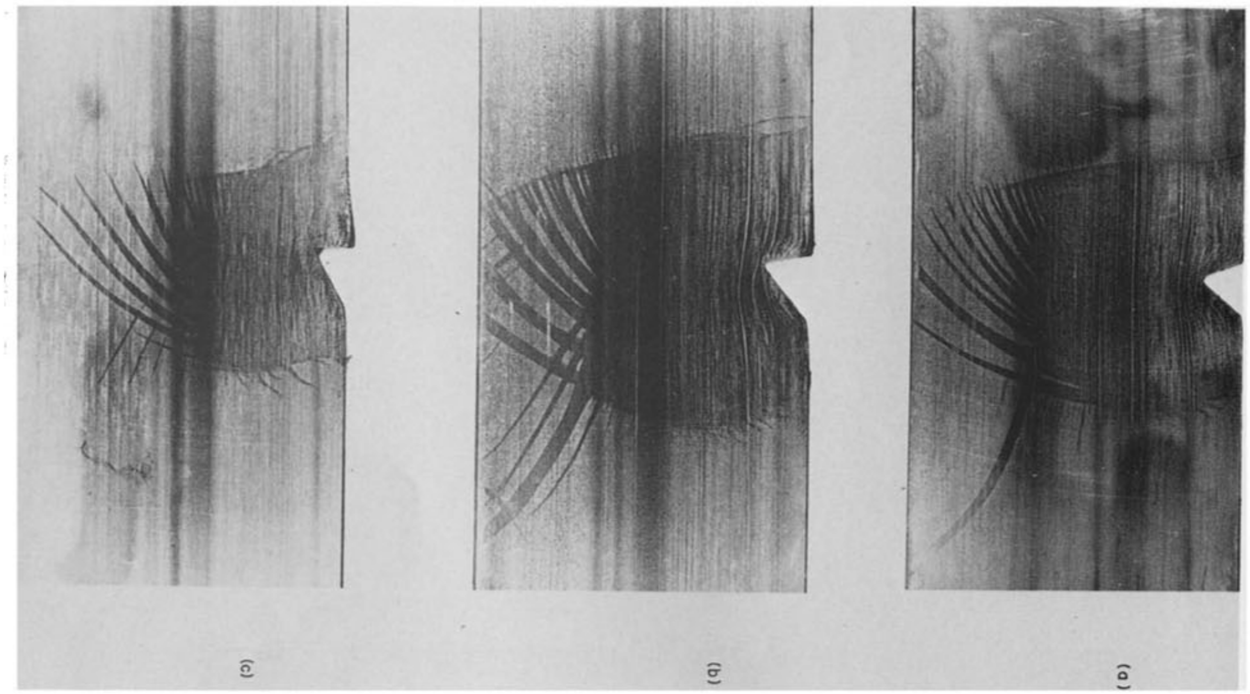

Despite the rotation of the wedge, the extent of the plastic strain field between the top and the bottom is similar.

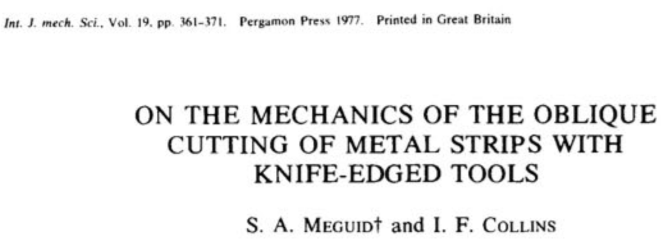

Task 1.2.2 (3/3) : Preliminary FEA work for MMT – Bai

Limitations

- Tip rigidity and fixed height in the model likely make cutting easier than in reality
- Plane strain condition also limits plastic zone.
- Bai et al. used a coefficient of friction of only 0.1 which is a significant underestimation for the materials that can be used for the testing

Conclusions

- FEA can be done, but significant work is needed to make sure it is reliable.
- Insight into the pre -strain field suggests that analytical modeling can be valuable

Task 1.2.3: Completed: Initial physical modeling

MMT's first analytical physical model is nearly finalized. Additional analytical models are planned for the near future. Analytical models may be used in lieu of, or to supplement, FEA for the development of final predictive models.

Basis of model:

- Prior to crack initiation the BTM performs what is essentially a "miniature tensile test" (right)
- Once the crack is initiated, we are left with an elongated ligament which can be used to calculate strain at failure with initial undeformed length (gage length) approximately equal to the blade radius.

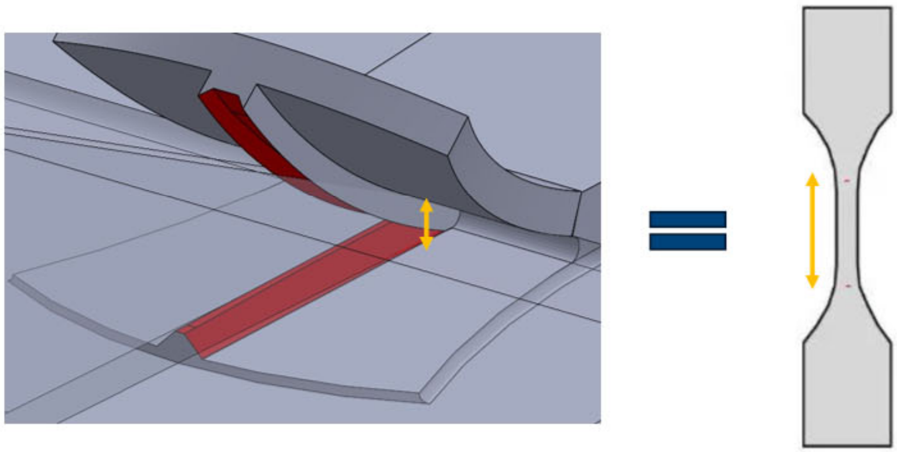

The rounded blade tip cuts a ligament with known "gage length" which is pulled apart in tension until fracture is initiated

Task 1.2.3: Completed: Initial physical modeling

- A physical model was developed which uses the HSD and BTM to predict the entire stress and strain curve to fracture for the purpose of calculating the Modulus of Toughness, or area under the stress vs. strain curve (right)
- The HSD predicts the stress vs. strain curve up to the ultimate tensile strength and the BTM is utilized to predict stress and strain at fracture
- The BTM predicts strain at fracture with the following formula:

$$\varepsilon_{fracture} = \ln\left(\frac{peak\ ligament\ height}{initial\ ligament\ height}\right)$$

- Stress at fracture is predicted by the following formula (Arasaratnam et al. 2011):

$$\sigma_{fracture} = \sigma_{uts}\left[w\left(\frac{\varepsilon_{fracture}}{\varepsilon_{uts}}\right)^{n} + (1-w)\left(1+\varepsilon_{fracture}-\varepsilon_{uts}\right)\right]$$

where w is a material dependent parameter equal to 0.5 and n is the strain hardening exponent

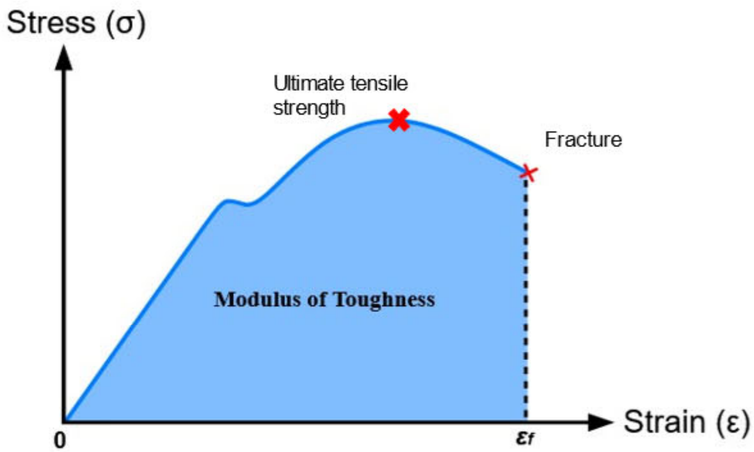

The **Modulus of Toughness** is the amount of energy per unit volume that a material can absorb before it fractures

Modulus of toughness Formula

$$\frac{\text{Energy}}{\text{Volume}} = \int_0^{\varepsilon_f} \sigma \, d\varepsilon$$

Task 1.2.3: Completed: Initial physical modeling

The plot to the right shows the results of the above-described predicted model vs. fracture toughness K values ($ksi\sqrt{in}$) performed on the same material in accordance with ASTM E1820. The correlation between the physical model and the laboratory testing is shown by $R^2 = 0.67$. Note that R2 is only 0.13 when the raw output parameter is used by itself.

Note: Validation and development of physical models and data analytics are ongoing.

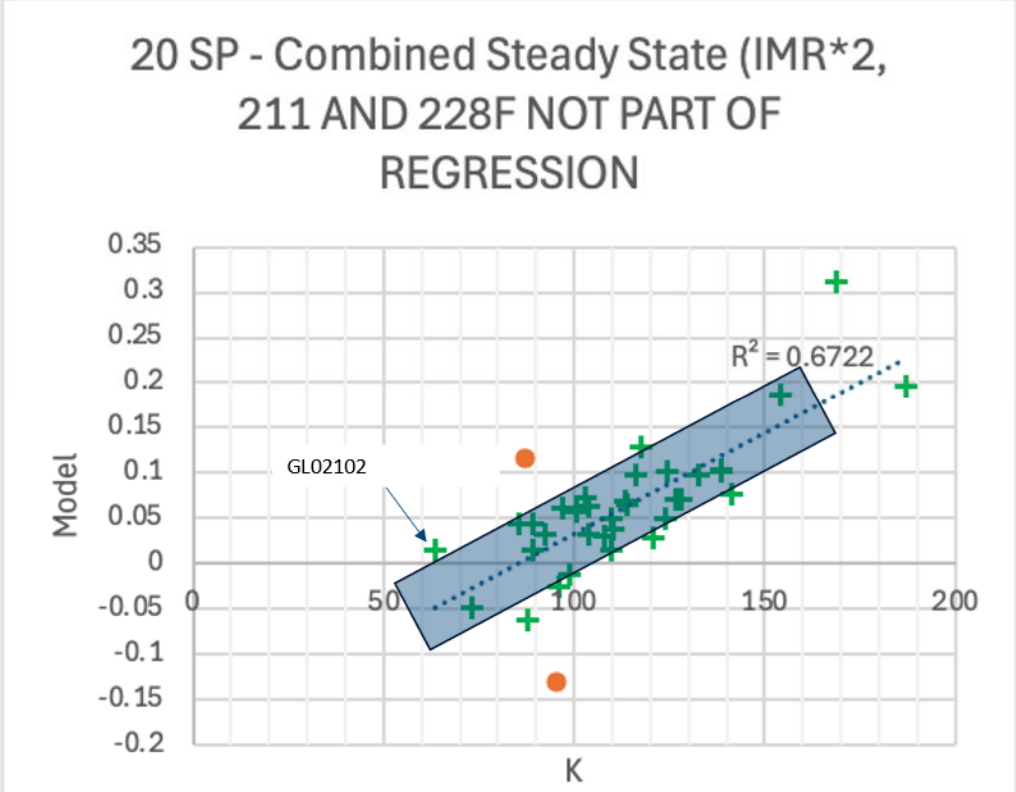

+/- 20 KSI (IN)1/2 [90+ PCT COVERAGE]

Task 1.2.3: Completed: Notes on laboratory testing

- All destructive laboratory testing is conducted in accordance with ASTM E1820, compact tension (CT) specimen geometry
- Analysis of destructive laboratory data has been an unexpected challenge due to lab-to-lab variation
- We discovered the variation through CVN to K conversions
- We have had to send specimens from a single sample to multiple labs to quantify variation

Conclusions

- We are currently investigating any variation between labs greater than 10%
- There is more work to gain better understanding of critical lab testing parameters and how to potentially flag bad lab results

Task 1.2.4 (1/3): Additional review of material response during tests

Added task: Because FEA models will need detailed validation before being used, we added a task to determine what fracture behavior needs to be reproduced and what should be the trends based on the experiments

Schematic to the right:

- Blade is traveling left to right (transparent)
- Fracture surface of ligament is red
- Ligament
    - chip side is a 'cup' shape
    - Pipe side is a 'cone' shape

Example of trend: 2025 PPIM paper by MMT (Provided with this report) shows some trends.

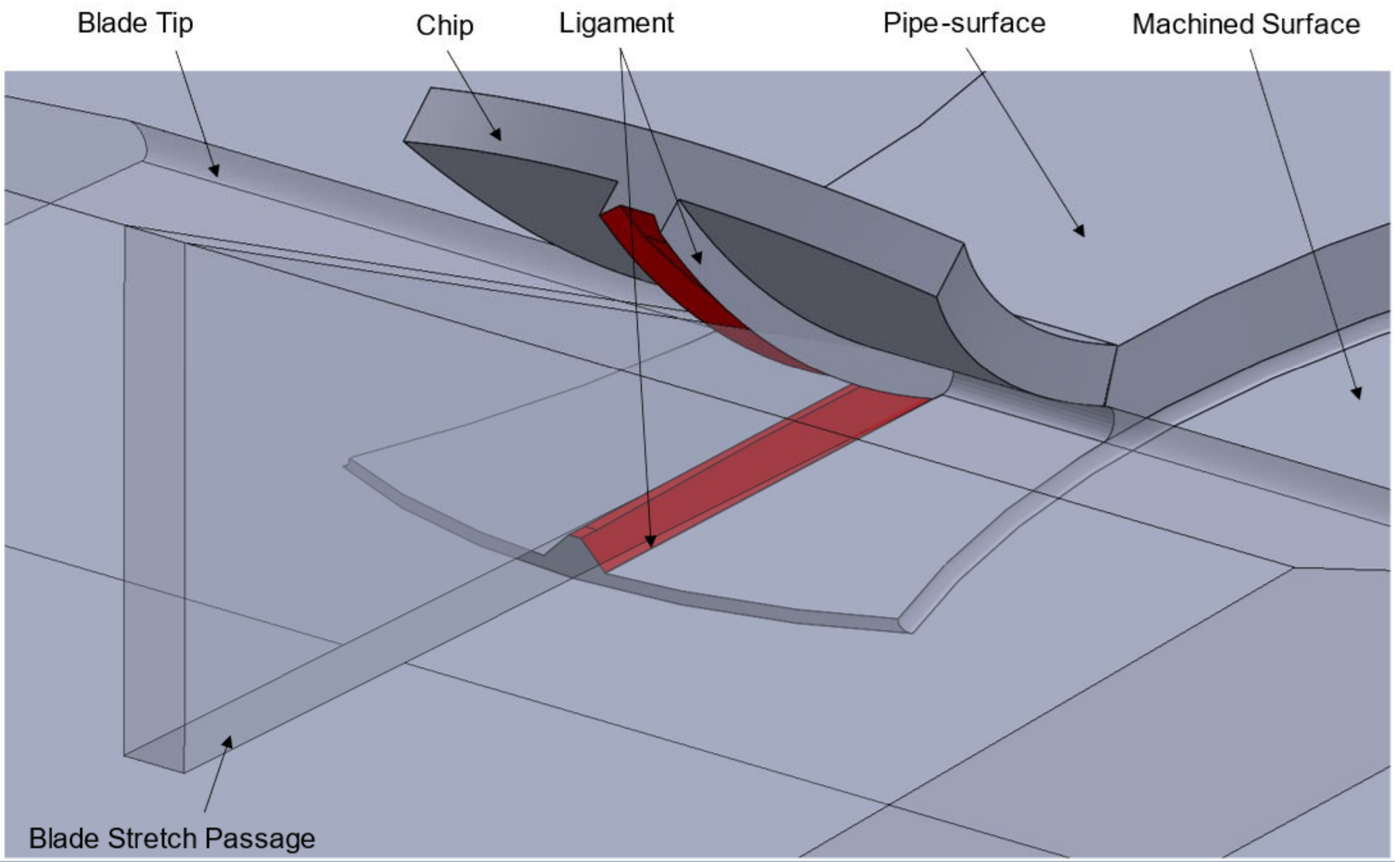

Task 1.2.4 (2/3): Additional review of material response during tests (Example)

Pipeline Pigging and Integrity Management Conference, Houston, January 2025

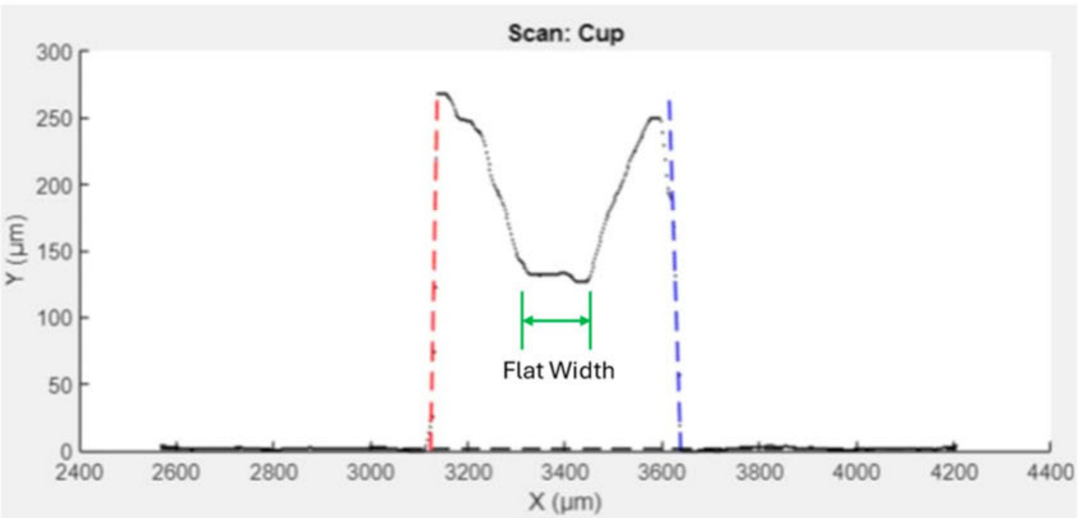

Figure 5. An Example of a Cup Ligament Profile and the Flat Width.

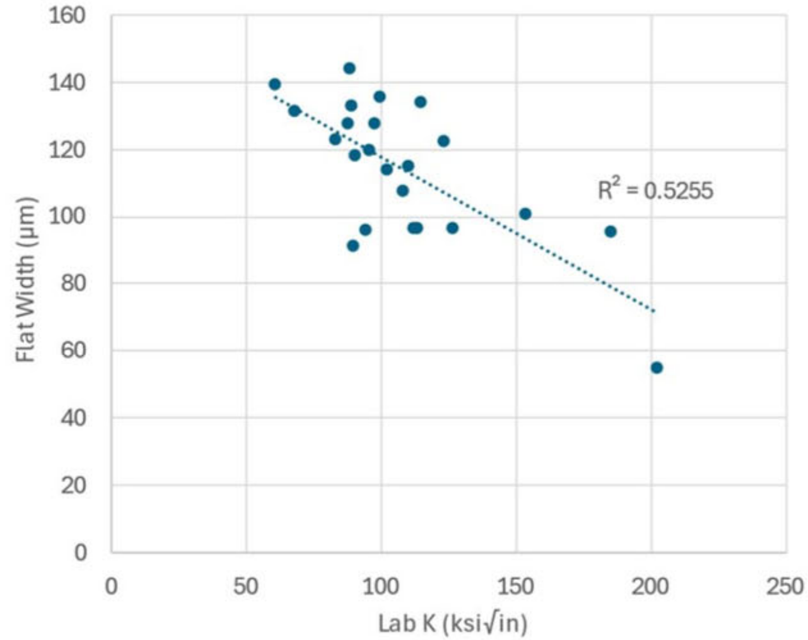

Figure 6. Correlation between Flat Width (x-axis) and Lab K (y-axis).

Task 1.2.4 (3/3): Additional review of material response during tests

New work moving forward :

- Tracking of strain on surface of test island
  - Utilize an etched or painted pattern on the test island surface which allows fine recreation of strain field
- Investigation of deformation in chip that gets separated from pipe
  - Deformation results in measurable change of thickness in chip
- Utilize polycarbonate to get insight into behavior in the sub surface of the test island
  - (Similar to the prior work with more variation in blade geometry and test parameters)
- Implement and collect load data for simulated materials

These items are intended for direct use validating FEA work product